Supporting Information

An Open-Shell Coronoid with Hybrid Chichibabin–Schlenk Conjugation

Bibek Prajapati, Duy-Khoi Dang, Piotr J. Chmielewski, Marcin A. Majewski, Tadeusz Lis, Carlos J. Gómez-García, Paul M. Zimmerman,* and Marcin Stępień*

ange_202109273_sm_miscellaneous_information.pdf

Table of Contents

Experimental

General. Tetrahydrofuran and 1,4-dioxane were dried using a commercial solvent purification system. Dichloromethane was distilled from calcium hydride when used as a reaction solvent. All other solvents and reagents were used as received. Compound **10**[1] was prepared according to the modified literature procedure. ^{1}H NMR spectra were recorded on high-field spectrometers (^{1}H frequency 500.13 or 600.13 MHz), equipped with broadband inverse or conventional gradient probe heads. Spectra were referenced to the residual solvent signals (chloroform-d, 7.24 ppm, dichloromethane-d_2, 5.32 ppm). ^{13}C NMR spectra were recorded with ^{1}H broadband decoupling and referenced to solvent signals ([13]CDCl$_3$, 77.0 ppm, [13]CD$_2$Cl$_2$, 55.0 ppm). Two-dimensional NMR spectra were recorded with 2048 data points in the t_2 domain and upto 2048 in the t_1 domain with a 1.5 s recovery delay. All 2D spectra were recorded with gradient selection except for ROESY. ROESY spinlock time were 200 -100 ms, respectively. High resolution mass spectra were recorded using MALDI and ESI ionization in the positive mode on Bruker Apex ultra-FT-ICR. UV-Vis-NIR Absorption spectrometry was performed using Perkin Elmer LAMBDA 1050 UV-NIR spectrometer. Electrochemical measurements (DCM, 0.1 M [NBu$_4$][PF$_6$], 293 K) were performed on an Metrohm Autolab potentiostat/galvanostat using a glassy carbon working electrode, platinum wire as the auxiliary electrode, and silver wire as a reference electrode. The voltammograms were referenced against the half-wave potential of Fc$^+$/Fc.

X-ray crystallography. X-Ray quality crystals of compound **8** were grown by slow evaporation method from toluene and methanol. Diffraction data were collected on a Rigaku Oxford Diffraction XtaLAB Synergy-R DW diffractometer equipped with a HyPix ARC 150° Hybrid Photon Counting (HPC) detector using CuKα (λ = 1.5418 Å) for compound **8** at 100 K. Data collection, cell refinement, data reduction and analysis were carried out with the Xcalibur PX software, CRYSALIS CCD and CRYSALIS RED, respectively (Oxford Diffraction Ltd., Abignon, England, 2009). An analytical absorption correction was applied with the use of CRYSALIS RED. All structures were solved by direct methods with the SHELXS-97 program and refined using SHELXL-97 with anisotropic thermal parameters for non-H atoms. In the final refinement cycles, all H atoms were treated as riding atoms in geometrically optimized positions. CCDC 2087057 (polymorph **A**) and 2087056 (polymorph **B**) contain the supplementary crystallographic data for this paper. These data are provided free of charge by The Cambridge Crystallographic Data Centre via www.ccdc.cam.ac.uk/data_request/cif

Magnetic measurements. Variable temperature susceptibility measurements were carried out with a Quantum Design MPMS-XL-7 SQUID magnetometer, in the temperature range 2–370 K, with an applied magnetic field of 0.5 T, on polycrystalline samples of compounds **8** and **9**, sealed in glass capillaries under inert atmosphere. The samples were measured in heating and cooling scans at a scan rate of 2 K/min. The data (and the fits) were very similar in the cooling and heating scans. The susceptibility data were corrected for the empty glass capillary previously measured using the same conditions and for the diamagnetic contribution of the samples as deduced by using Pascal´s constant tables.[2]

Computational methods. Density functional theory (DFT) calculations were performed using Gaussian 16.[3] DFT geometry optimizations were carried out in unconstrained C_1 symmetry, using molecular mechanics or semiempirical models as starting geometries. The calculations were performed using the hybrid functional B3LYP,[4–6] including the CAM[7] and GD3BJ[8] corrections, and the 6-31G(d,p) basis set. Unrestricted wavefunctions were used for all open-shell systems and broken-symmetry solutions were obtained for all open-shell singlets. Each structure was optimized to meet standard convergence criteria, and the existence of a local minimum was verified by a normal mode frequency calculation. NICS maps (Figure 7) were obtained at the CAM level of theory, by evaluating GIAO shieldings over a

square grid of 201 × 201 points with an extent of 11 × 11 Å and located 1 Å above the plane of the molecule. ACID[9,10] calculations were performed using the code kindly provided by Prof. Reiner Herges and his group.

Optimized geometries of the singlet, triplet, quintet, and septet for coronoid **8'** were computed at the CASSCF(6,6)/cc-pVDZ level of theory[11,12] with the RICD approximation[13,14] in the OpenMolcas electronic structure package.[15] The singlet and septet optimizations yield D_{3h}-symmetric geometries, while C_{2v}-symmetric structures are found for the triplet and quintet. Subsequent RAS(6,6)-SF/cc-pVDZ[16,17] calculations provide insight into the radical character of **8'**. The polyradicaloid indices ($\gamma_0, \gamma_1, \gamma_2$) increase as the geometry of **8'** is optimized for increasing spin manifolds (Figure S1). Energies for the lowest eight spin states are reported in Figure S2 where there are two degenerate triplets and two degenerate quintets for the D_{3h} geometries. As the symmetry breaks from D_{3h} to C_{2v}, the degeneracy of these states lifts. This behavior can be explained by analyzing the radical sites and the spin Hamiltonian (Figure S3). The radical sites were identified to be six carbons (labeled in Figure S3) with the largest odd-electron density.
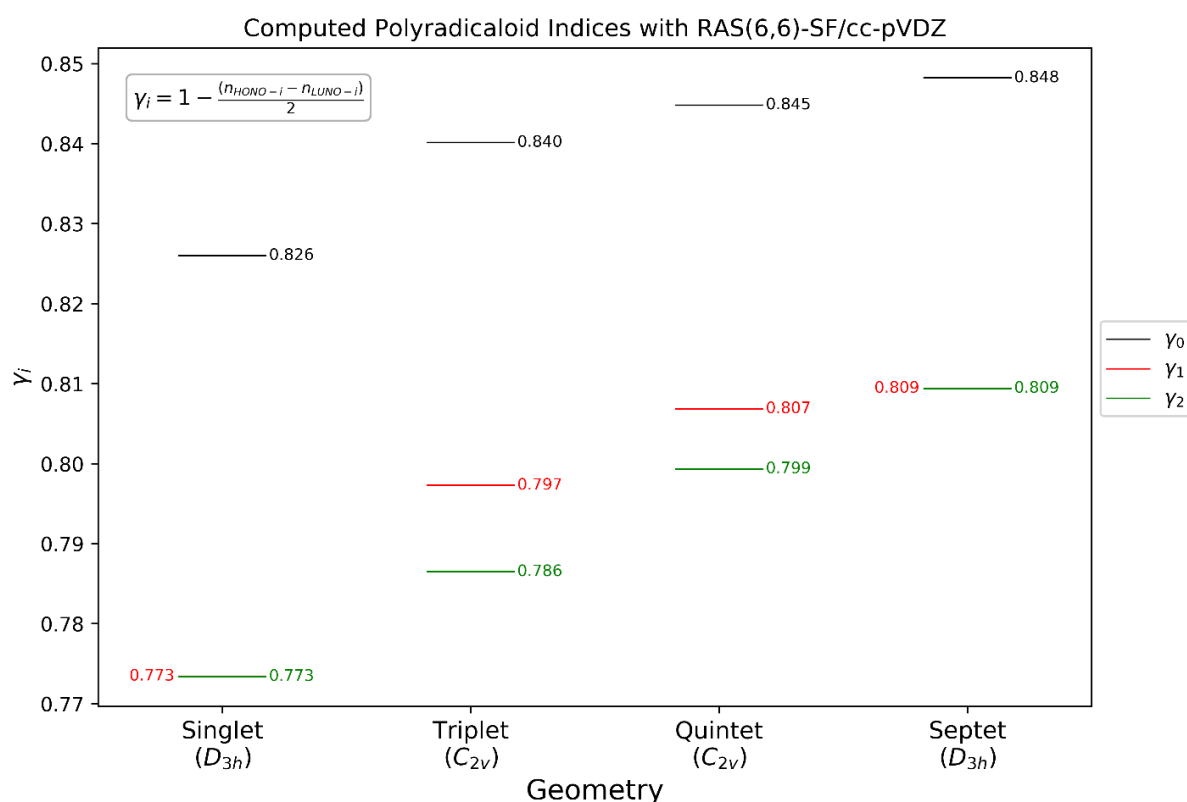

Figure S1. Polyradicaloid indices (γ_i) from RAS(6,6)-SF/cc-pVDZ are shown for the ground singlet electronic state at various optimized CASSCF(6,6)/cc-pVDZ geometries.

We first begin with an analysis of the spin Hamiltonian for the D_{3h} geometries, where $\varepsilon_i = 0$ for all i. Diagonalization of the D_{3h} spin Hamiltonian produces the following analytic expressions for the eigenvalues:

$$E_0 = J_1 + J_2 + 2J_3 + J_4,$$

$$E_1 = E_2 = -J_3 - \sqrt{J_1^2 - J_1 J_2 - J_1 J_4 + J_2^2 - J_2 J_4 + J_4^2},$$

$$E_3 = E_4 = -J_3 + \sqrt{J_1^2 - J_1 J_2 - J_1 J_4 + J_2^2 - J_2 J_4 + J_4^2},$$

$$E_5 = -J_1 - J_2 + 2J_3 - J_4.$$

To compute J_1 and J_2, the spin gap error between the D_{3h} eigenvalues and the RAS(6,6)-SF spin states are minimized, i.e. we minimize the following equation:

$$R = \sqrt{\frac{\sum_{i=1}^{5}\left(E_i^{SF} - E_i\right)^2}{5}}, \tag{1}$$

where E_i^{SF} corresponds to RAS(6,6)-SF energies and the ground state eigenvalue is assumed to be zero. Due to the difference in dimension of the spin Hamiltonian and RAS(6,6)-SF spin Hamiltonian, it is important to select the appropriate RAS(6,6)-SF spin states which have corresponding spin Hamiltonian eigenvalues. Since the non-degenerate triplet state (T_3) is higher in energy than the doubly degenerate set, it may be considered an excited triplet which is consistent with the higher number of unpaired electrons in T_3 as discussed in the main text. Furthermore, since there are two sets of doubly degenerate eigenvalues in the spin Hamiltonian (one corresponding to a set of triplets and the other a set of quintets), Equation (1) is minimized against the sets of doubly degenerate triplets and quintets computed from RAS(6,6)-SF in each D_{3h} geometry. The resulting couplings and RMSE are reported in Table S1.
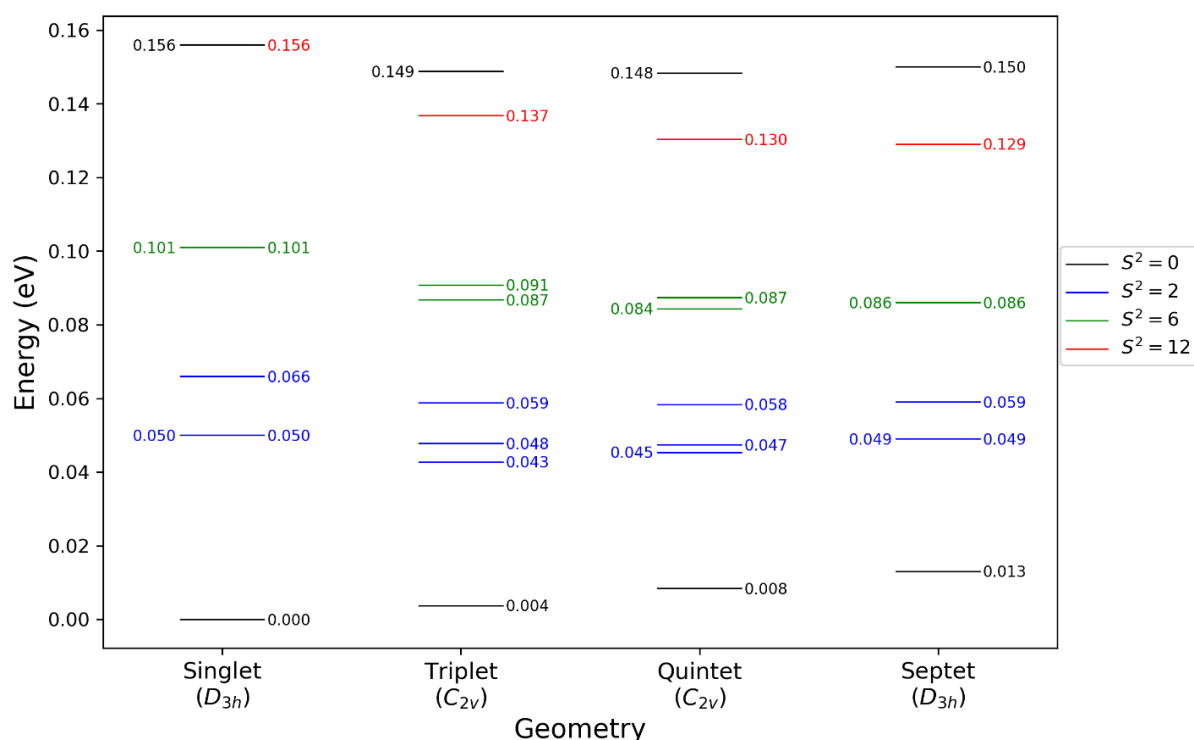

Figure S2. RAS(6,6)-SF/cc-pVDZ energies and spins (S^2) of the first eight states of **8'** are shown for various optimized CASSCF(6,6)/cc-pVDZ geometries. The singlet D_{3h} geometry has a 6-fold degeneracy at 0.156 eV between an additional two singlet and two triplet states.

One might consider the possibilities of J_i having different signs and could start the minimization of Equation (1) at various points to find other minima with different signs for J_i, however these result in

RMSE several orders of magnitude higher than those reported in Table S1. This suggests that the J_i should all have the same sign. In the case of all the J_i being positive, the RMSE remains the same, however the eigenvalue $-J_1 - J_2 + 2J_3 - J_4$ corresponds to the septet state. Having all positive J_i would consequentially place the septet as the ground state. Therefore, the assignment of negative sign for J_i in the D_{3h} case gives antiferromagnetic coupling for the ground state. The S_0 eigenvector of the D_{3h} spin Hamiltonian has uniform magnitudes indicating a single spin alignment.

A.

	1	2	3	4	5	6
1		$-(J_1 + \varepsilon_1)$	$-(J_3 + \varepsilon_{3a})$	$-J_4$	$-J_3$	$-J_2$
2	$-(J_1 + \varepsilon_1)$		$-J_2$	$-J_3$	$-J_4$	$-(J_3 + \varepsilon_{3a})$
3	$-(J_3 + \varepsilon_{3a})$	$-J_2$		$-J_1$	$-(J_3 + \varepsilon_{3b})$	$-(J_4 + \varepsilon_4)$
4	$-J_4$	$-J_3$	$-J_1$		$-(J_2 + \varepsilon_2)$	$-(J_3 + \varepsilon_{3b})$
5	$-J_3$	$-J_4$	$-(J_3 + \varepsilon_{3b})$	$-(J_2 + \varepsilon_2)$		$-J_1$
6	$-J_2$	$-(J_3 + \varepsilon_{3a})$	$-(J_4 + \varepsilon_4)$	$-(J_3 + \varepsilon_{3b})$	$-J_1$	

B. C.
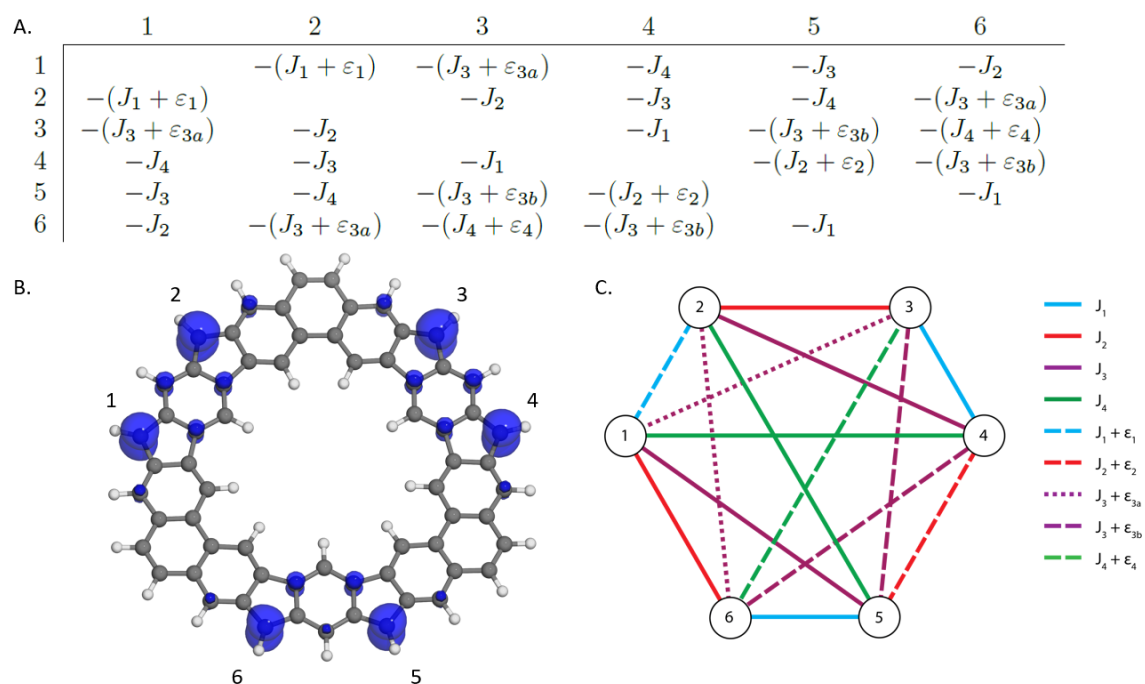
Figure S3. The odd-electron density (isovalue = 0.005 a.u.) of the optimized singlet geometry (left) and corresponding spin Hamiltonian (right) are shown with the six radical sites labeled. For the D_{3h} geometries, $\varepsilon_1 = \varepsilon_2 = 0$ due to symmetry.

Table S1. Computed spin couplings for **8'** (eV).

Geometry	J_1^a	J_2^a	J_3^a	J_4^a	ε_1^b	ε_2^b	ε_{3a}^b	ε_{3b}^b	ε_4^b	RMSE
Singlet (D_{3h})	-0.0382	-0.0302	-0.0008	-0.0097	0	0	0	0	0	1.70E-7
Triplet (C_{2v})	-0.0322	-0.0262	-0.0011	-0.0081	0.0101	-0.0097	-0.0007	0.0003	0.0042	6.31E-9
Quintet (C_{2v})	-0.0295	-0.0240	-0.0011	-0.0076	-0.0053	-0.0095	-0.0004	0.0004	-0.0017	1.03E-9
Septet (D_{3h})	-0.0277	-0.0233	-0.0012	-0.0073	0	0	0	0	0	5.25E-7

[a] Computed spin coupling constant. [b] Perturbation to spin coupling due to C_{2v} geometry.

Similar analysis can be applied to the C_{2v} geometries, but eigenvalue decomposition of the spin Hamiltonian for the C_{2v} geometries must be done numerically. For the C_{2v} geometries, the two triplet states lowest in energy (see Figure S2) are chosen for minimizing Equation (1). The C_{2v} Hamiltonian is minimized in two separate steps. First, it is treated with a D_{3h} Hamiltonian to obtain the initial J_i, then Equation (1) is minimized to compute the ε_i with fixed J_i. In other words, the C_{2v} Hamiltonian is treated

as a perturbed D_{3h} Hamiltonian. The resulting J_i and ε_i are reported in Table 1 along with couplings from the D_{3h} geometries.

Finally, we answer the question of spin alignment for the C_{2v}. Unlike the D_{3h} case, the singlet eigenvector for each of the C_{2v} spin Hamiltonians has non-uniform magnitudes indicating multiple spin alignments are involved. By pairing the spins across the vertical mirror plane (i.e. pairs 1-2, 3-6, 4-5 with ordering from Figure S3), the overall spin system can be treated as a trimer of paired spins and the singlet eigenvector for the two C_{2v} spin Hamiltonians can then be decomposed as a linear combination of multiple spin products.[18] The resultant singlet wave function at the triplet and quintet geometries are then, respectively,

$$\psi_3 = 0.600\psi_{\uparrow\downarrow\uparrow\downarrow\uparrow\downarrow} + 0.292\psi_{\downarrow\uparrow\uparrow\downarrow\uparrow\downarrow} + 0.212\psi_{\uparrow\downarrow\downarrow\downarrow\uparrow\uparrow} + 0.095\psi_{\uparrow\downarrow\uparrow\uparrow\downarrow\downarrow},$$

$$\psi_5 = 0.607\psi_{\uparrow\downarrow\uparrow\downarrow\uparrow\downarrow} + 0.136\psi_{\downarrow\uparrow\uparrow\downarrow\uparrow\downarrow} + 0.198\psi_{\uparrow\downarrow\downarrow\downarrow\uparrow\uparrow} + 0.274\psi_{\uparrow\downarrow\uparrow\uparrow\downarrow\downarrow},$$

where radical site ordering follows that of Figure S3. In other words, the ground state singlet wavefunctions for the C_{2v} geometries are superpositions of multiple singlet spin alignments in this spin Hamiltonian model.

Synthesis
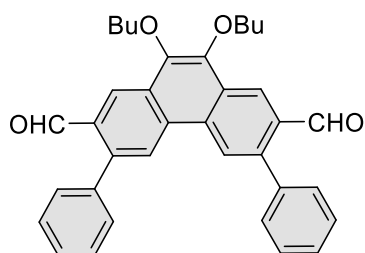
9,10-Dibutoxy-3,6-diphenylphenanthrene-2,7-dicarbaldehyde (S1). Compound **10** (150 mg, 0.28 mmol)and phenyl boronic acid (89.75 mg, 0.7 mmol) was dissolved in 27 mL of dioxane and the solution was purged with nitrogen for 15 minutes. The degassed solution of sodium carbonate (237.18 mg, 2.24 mmol) in 3 mL of water was added to the mixture followed by the addition of tetrakis(triphenylphosphine)palladium(0) (32.32 mg, 0.028 mmol) The mixture was purged with nitrogen for few minutes and heated at 100 °C for overnight. After cooling to room temperature, water was added and extracted with dichloromethane. The organic layer was washed with brine, dried over anhydrous sodium sulfate(VI) and the solvent was removed on rotary evaporator. The crude mixture was purified via silica column chromatography using 20% ethyl acetate in *n*-hexane as an eluent to give compound **S2** (145 mg, 98%) as a yellow solid. **¹H NMR** (500 MHz, chloroform-*d*, 300 K): δ 10.16 (2H, s), 8.93 (2H, s,), 8.63 (2H, s,), 7.50 (10H, m) 4.29 (4H, t, ^3J = 6.8 Hz), 1.94 (4H, m), 1.63 (4H, m), 1.04 (6H, t, ^3J = 7.4 Hz). **¹³C NMR** (125 MHz, chloroform-*d*, 300 K): δ 192.11, 143.97, 141.64, 138.04, 133.02, 130.32, 130.26, 128.56, 128.16, 125.86, 123.68, 73.77, 32.43, 19.39, 13.97. **HRMS** (ESI–TOF): *m/z*: [M + Na]+ Calcd for $C_{36}H_{34}O_4$: 553.2349; Found 553.2317.
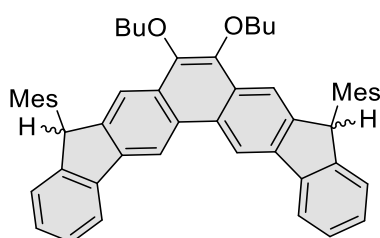
7,8-Dibutoxy-5,10-dimesityl-5,10-dihydrodiindeno[2,1-b:1',2'-h]phenanthrene (S2). Compound **S1** (100 mg, 0.188 mmol) was dissolved in dry tetrahydrofuran (20 mL) in a flame-dried Schlenk flask and purged with nitrogen for 15 minutes. 2-mesitylmagnesium bromide (0.75 mL, 1 M in THF, 0.754 mmol) was added dropwise at room temperature and stirred overnight under nitrogen. The mixture was quenched with water, extracted with dichloromethane, dried over anhydrous sodium sulfate(VI) and evaporated to dryness. The resulting solid was dissolved in freshly distilled dichloromethane (15 mL) and purged with nitrogen for 15 minutes. Several drops of borontrifluoride diethyl etherate were added slowly and stirred for 15 minutes at room temperature. The solvent was removed on a rotary evaporator and the crude mixture was purified via silica column chromatography using 20% dichloromethane in *n*-hexane as an eluent to give compound **S3** as a colorless solid (131 mg, 95%, mixture of stereoisomers). **¹H NMR** (500 MHz, chloroform-*d*, 300 K): δ 9.21 (2H, s), 8.15 (2H, d, ^3J = 7.7 Hz), 8.03 (2H, s,), 7.49 (2H, t, ^3J = 7.4 Hz), 7.31 (4H, m), 7.04 (2H,s), 6.63 (2H,s), 5.71 (2H, s) 4.11 (4H, m), 2.73 (6H, s), 2.27 (6H, s), 1.70 (4H, m), 1.42 (4H, m), 1.10 (6H, s), 0.85 (6H, t, ^3J = 7.4 Hz). **¹³C NMR** (125 MHz, chloroform-*d*, 300 K): δ 147.98, 146.09, 143.38, 140.83, 139.29, 137.74, 137.56, 136.10, 134.23, 130.58, 129.24, 128.73, 128.32, 127.66, 127.02, 124.47, 120.43, 117.43, 113.46, 73.27, 49.58, 32.38 21.73, 20.83, 19.42, 18.98, 13.74. **HRMS** (ESI–TOF): *m/z*: [M + Na]+ Calcd for $C_{54}H_{54}O_2$: 757.4016; Found 757.3967.
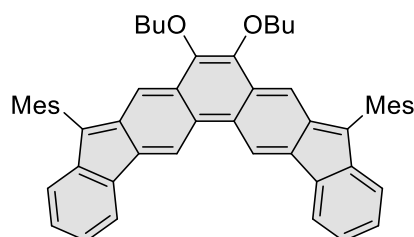
7,8-Dibutoxy-5,10-dimesityldiindeno[2,1-b:1',2'-h]phenanthrene (9). Compound **S2** (50 mg, 0.068 mmol) was dissolved in dry tetrahydrofuran (15 mL) in a flame-dried Schlenk flask and purged with nitrogen for 15 minutes. Potassium *tert*-butoxide solution (2 mol/L in 2-MeTHF, 102 μL, 0.204 mmol) was added slowly to the vigorously stirred solution at room temperature. The mixture was stirred for 5 minutes and a diiodine solution (0.1 M in THF, 748 μL, 74.8 μmol) was added dropwise with stirring. The dark-red mixture was stirred at room temperature for 10 minutes. The mixture was quenched with water, treated with 0.1 N HCl and extracted with dichloromethane. The organic layer was washed with brine, dried over anhydrous sodium sulfate(VI) and the solvent was removed on a rotary evaporator. The crude mixture was purified via neutral silica column chromatography using 1:5 DCM/*n*-hexane as an eluent to afford compound **9** as a dark blue solid (41 mg, 82%).

Method 2: Compound **S2** (20 mg, 0.027 mmol) was dissolved in freshly distilled dichloromethane (10 mL) in a flame-dried Schlenk flask and purged with nitrogen for 15 minutes. 2,3-Dichloro-5,6-dicyanobenzoquinone (18.91 mg, 0.082 mmol) was added and the mixture was stirred under nitrogen at an ambient temperature for 2 hours. The mixture was passed through a short plug of alumina and washed with hot methanol to give compound **9** as a dark blue solid (14 mg, 70%) **^{1}H NMR** (500 MHz, dichloromethane-d_2, 190 K): δ 8.45 (2H, s), 7.77 (2H, d, ^3J = 7.30 Hz), 7.15 (4H, m,), 7.08 (2H, t, ^3J = 7.57 Hz), 6.98 (4H, s), 6.81 (2H,d, ^3J = 7.42 Hz), 3.90 (4H,t, ^3J = 6.80 Hz), 2.31 (6H, s), 2.06 (12H, s), 1.55 (4H, m), 1.26 (4H, m), 0.77 (6H, t, ^3J = 7.4 Hz). **^{13}C NMR** (125 MHz, dichloromethane-d_2, 190 K): δ 142.40, 142.28, 141.94, 139.05, 137.40, 136.96, 136.56, 135.14, 130.15, 129.56, 128.15, 127.94, 126.82, 122.15, 120.87, 117.12, 117.03, 72.47, 31.88, 20.85, 20.31, 19.47, 13.70. **HRMS** (ESI–TOF): *m/z*: [M]$^+$ Calcd for $C_{54}H_{52}O_2$: 732.3962; Found 732.3992.
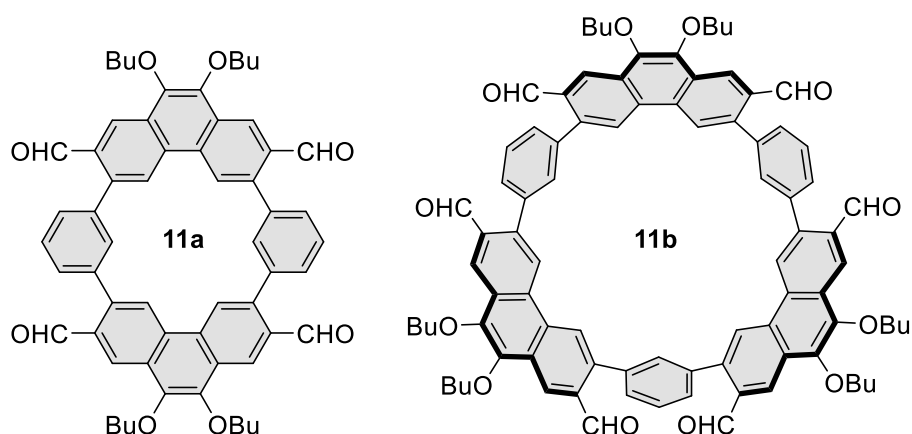
Compound (11). Compound **10** (300 mg, 0.559 mmol) and 1,3-phenylenediboronic acid (95.59 mg, 0.559 mmol) was dissolved in dioxane (150 mL) and the solution was purged with nitrogen for 15 minutes. The degassed solution of potassium carbonate (772.57 mg, 5.59 mmol) in water (15 mL) was added to the mixture followed by the addition of tetrakis(triphenylphosphine)palladium(0) (129.29 mg, 0.112 mmol) The mixture was purged with nitrogen for a few minutes and refluxed for 48 hours.

After cooling to room temperature, water was added and extracted with dichloromethane. The organic layer was washed with brine, dried over anhydrous sodium sulfate(VI) and the solvent was removed on a rotary evaporator. The crude mixture was purified via silica column chromatography using 70% dichloromethane in *n*-hexane as an eluent to give the dimer compound **11a** (36 mg, 14%) and trimer compound **11b** (23 mg, 9%) as yellow solids.

Compound **11a**: **^{1}H NMR** (500 MHz, chloroform-*d*, 300 K): δ 10.57 (4H, s), 9.10 (4H, s), 8.99 (4H, s), 8.30 (4H, s), 7.60 (12H, m), 4.33 (8H,t, ^3J = 6.80 Hz), 1.96 (8H, m), 1.65 (8H, m), 1.05(12H, t, ^3J = 7.4 Hz). **^{13}C NMR** (151 MHz, chloroform-*d*, 300 K): δ 191.76, 144.31, 140.54, 139.47, 132.55, 131.48, 130.85, 130.79, 130.53, 127.90, 127.59, 124.63, 73.87, 32.43, 19.38, 13.96. **HRMS** (ESI–TOF): *m/z*: [M + Na]$^+$ Calcd for $C_{60}H_{56}O_8$: 927.3867; Found 927.3910.

Compound **11b**: **^{1}H NMR** (500 MHz, chloroform-*d* , 300 K): δ 10.30 (6H, s), 8.94 (6H, s), 8.52 (6H, s), 7.58 (6H, m), 7.49 (6H, m), 4.30 (12H,t, ^3J = 6.80 Hz), 1.94 (12H, m), 1.63 (12H, m), 1.04(18H, t, ^3J = 7.4 Hz). **^{13}C NMR** (125 MHz, chloroform-*d*, 300 K): δ 191.54, 144.08, 143.94, 140.64, 138.71, 138.58, 133.03, 132.93, 131.00, 130.68, 130.65, 130.33, 129.87, 128.83, 128.57, 126.42, 125.02, 124.54, 73.84, 32.42, 31.57, 22.64, 19.39, 14.10, 13.96. **HRMS** (MALDI–TOF): *m/z*: [M + Na]$^+$ Calcd for $C_{90}H_{84}O_{12}$: 1379.5855; Found 1379.6262.
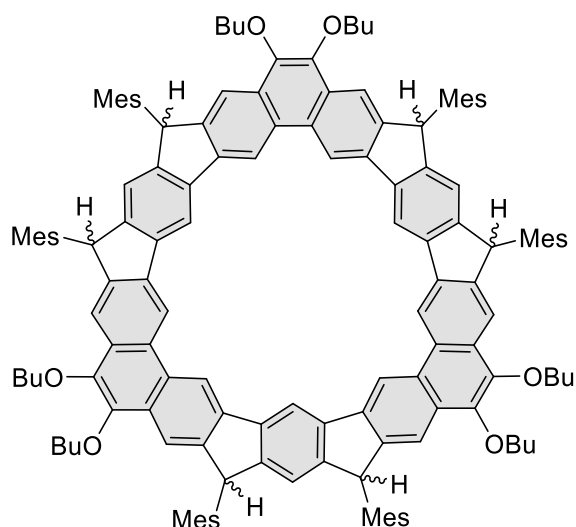
Compound (12). Trimer compound **11b** (25 mg, 0.0184 mmol) was dissolved in dry tetrahydrofuran (20 mL) in a flame-dried Schlenk flask and purged with nitrogen for 15 minutes. 2-Mesitylmagnesium bromide (1.10 mL, 1 M in THF, 1.10 mmol) was added dropwise at room temperature and stirred overnight under nitrogen. The mixture was quenched with water, extracted with dichloromethane, dried over anhydrous sodium sulfate(VI) and evaporated to dryness. The resulting solid was dissolved in freshly distilled dichloromethane (15 mL) and purged with nitrogen for 15 minutes. A few drops of boron-trifluoride diethyl etherate was added slowly and stirred for 15 minutes at room temperature. The solvent was removed on rotary evaporator and the crude mixture was purified via silica column chromatography using 25% dichloromethane in n-hexane as an eluent to give compound **12** as a beige solid (26 mg, 72%, mixture of stereoisomers). **^{1}H NMR** (500 MHz, chloroform-*d*, 300 K): δ 9.41 (6H, m), 8.93 (3H, m), 8.07 (6H, m), 7.35 (3H, m), 7.01 (6H, m), 6.61 (6H, m), 5.73 (6H, m), 4.08 (12H,m), 2.73

(18H, m), 2.25 (18H, m), 1.66 (12H, m), 1.40 (12H, m), 1.32 (12H, m), 0.86 (18H, m). **^{13}C NMR** (125 MHz, chloroform-*d*, 300 K): δ 149.75, 149.50, 149.39, 149.19, 149.12, 148.92, 146.65, 146.61, 146.49, 142.73, 142.69, 140.66, 140.45, 140.33, 139.73, 139.62, 139.56, 137.66, 136.06, 134.51, 134.46, 134.43, 130.74, 129.11, 129.06, 128.82, 128.78, 120.91, 117.96, 117.92, 117.84, 113.76, 73.30, 48.97, 48.92, 48.81, 32.43, 21.80, 21.73, 20.81, 19.51, 19.48, 19.14, 19.09, 19.05, 13.86. **MS** (MALDI–TOF): *m/z*: [M − H]$^+$ Calcd for $C_{144}H_{144}O_6$: 1968.6222; Found 1968.0879.
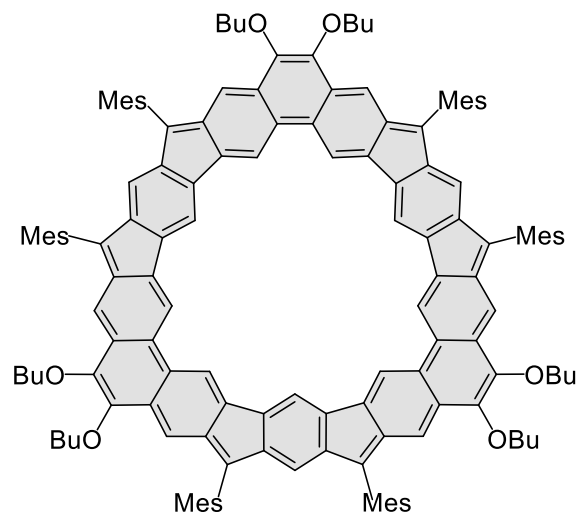
Compound (8). Method 1: Compound **12** (20 mg, 0.010 mmol) was dissolved in dry tetrahydrofuran (15 mL) in a flame-dried Schlenk flask and purged with nitrogen for 15 minutes. Potassium *tert*-butoxide solution (2 mol/L in 2-MeTHF, 91.5 μL, 0.183 mmol) was added slowly to vigorously stirred solution at room temperature. The mixture was stirred for 5 minutes and diiodine solution(0.1 M in THF, 609 μL, 60.9 μmol) was added dropwise to the stirred solution. The dark-red mixture was stirred at room temperature for 10 minutes. The mixture was quenched with water, treated with 0.1 N HCl and extracted with dichloromethane. The organic layer was washed with brine, dried over anhydrous sodium sulfate(VI) and the solvent was removed on a rotary evaporator. The mixture was passed through a short plug of alumina and washed with hot methanol to give compound **8** as a dark green solid (17 mg, 85%).

Method 2: Compound **12** (20 mg, 0.01 mmol) was dissolved in freshly distilled dichloromethane (10 mL) in a flame dried Schlenk flask and purged with nitrogen for 15 minutes. 2,3-Dichloro-5,6-dicyanobenzoquinone (14.10 mg, 0.06 mmol) was added and the mixture was stirred under nitrogen in an ambient temperature for 3 hours. The mixture was passed through short plug of alumina and washed with hot methanol to give a compound **8** as a dark green solid (13 mg, 65%). **^{1}H NMR** (600 MHz, dichlorofluoromethane-*d*, 160 K): δ 13.22 (2H, b), 12.52 (1H, b), 6.72 (4H, b), 6.22 (2H, b), 5.14 (1H, b), 3.59 (4H,b), 2.14 (6H, b), 1.90 (12H, b), 1.35 (4H, b), 0.98 (4H, b), 0.67 (6H, b). **HRMS** (MALDI–TOF): *m/z*: [M]$^+$ Calcd for $C_{144}H_{138}O_6$: 1963.0488; Found 1963.06383.

Additional Schemes
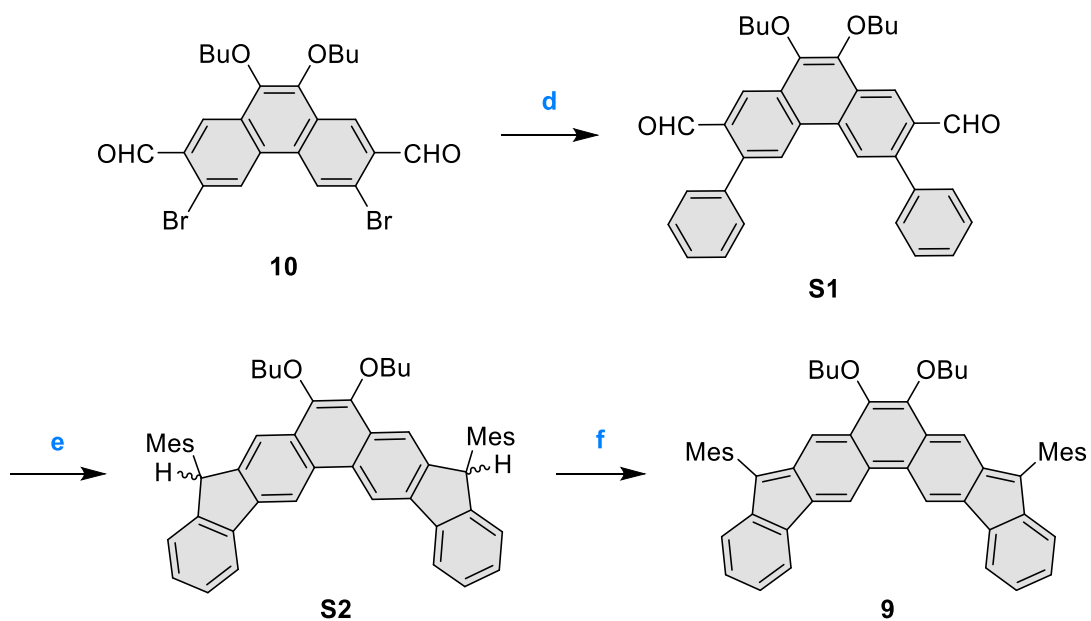
Scheme S2. Synthesis of compounds **S1**, **S2** and **9**. Reagents and conditions: d) phenylboronic acid (2.5 equiv), Pd(PPh$_3$)$_4$ (0.1 equiv), Na$_2$CO$_3$ (8.0 equiv), dioxane, H$_2$O; e) 1. 2-MesMgBr (1 M solution in THF, 4.0 equiv), THF, 2. BF$_3$·Et$_2$O, DCM; f) 1. *t*-BuOK (2 M in 2-MeTHF, 3.0 equiv), THF, 2. I$_2$ (0.1 M in THF, 1.0 equiv) or DDQ (4.0 equiv), DCM .
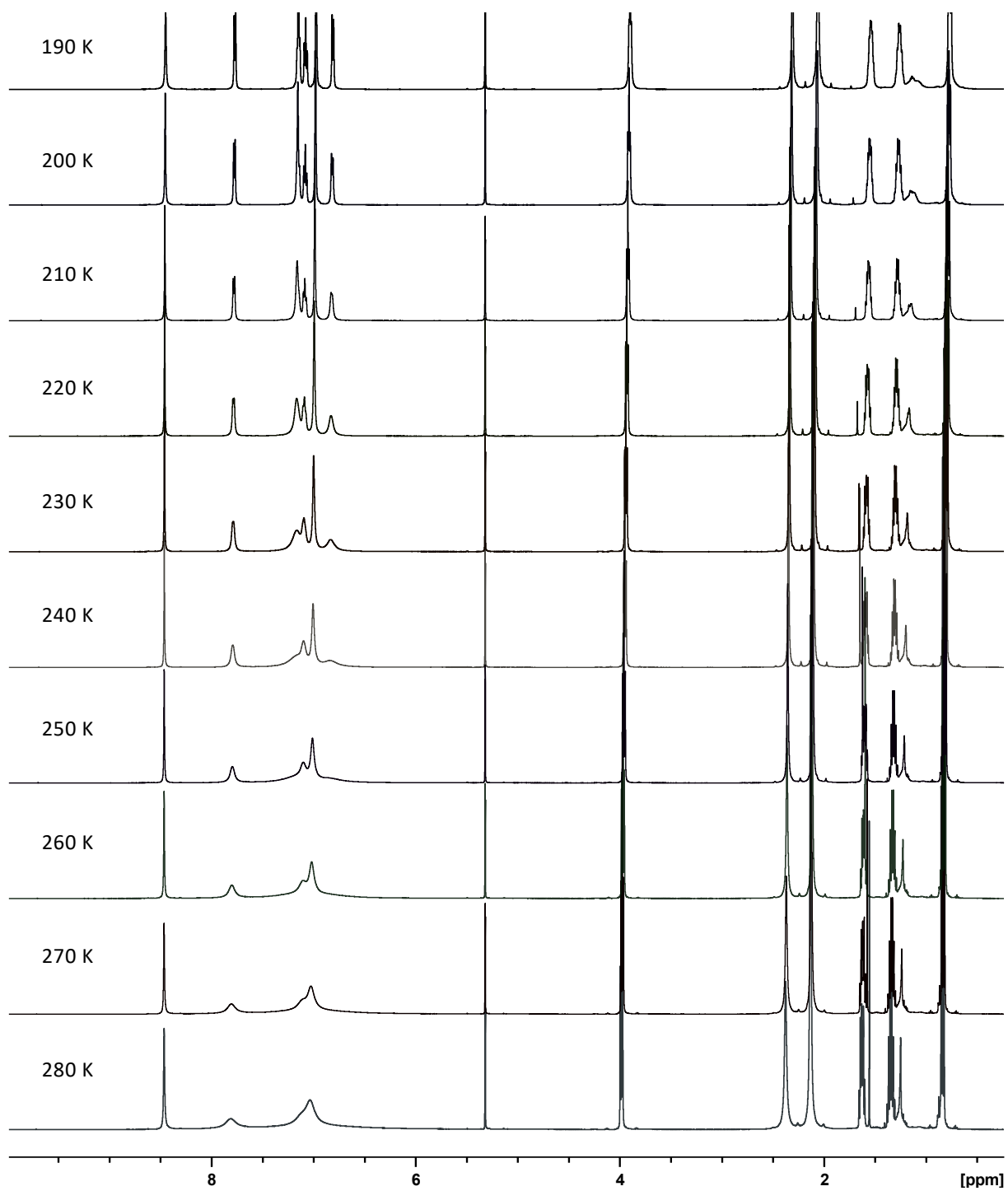
Additional Figures

Figure S4. Variable temperature ^1H NMR spectra of **9** (500 MHz, dichloromethane-d_2, 280-190 K).
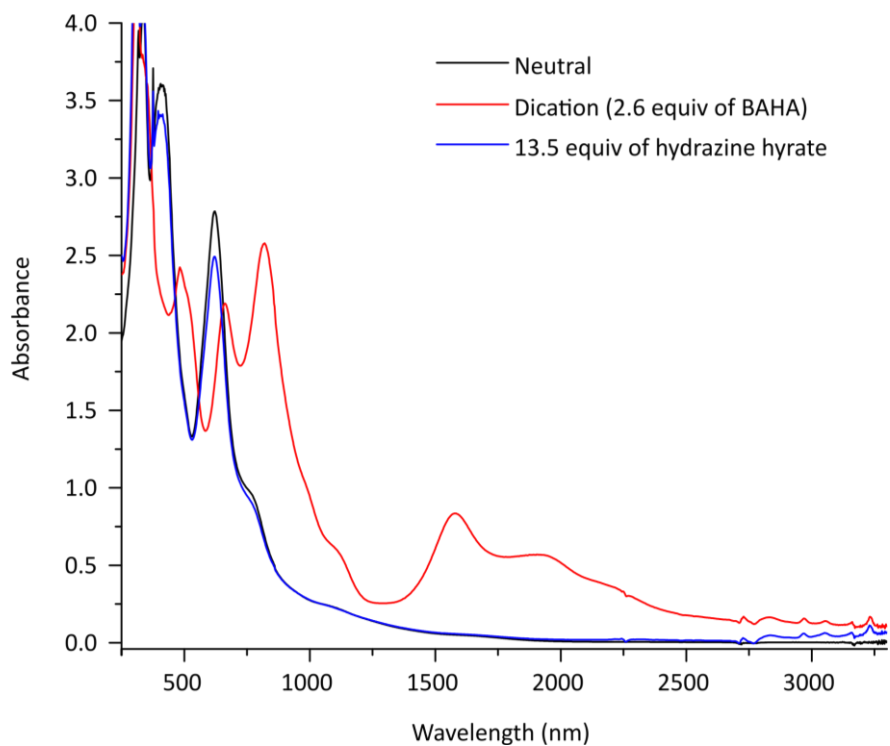
Figure S5. Reversibility of chemical oxidation investigated for **8**. Black line, neutral solution; red line, dicationic solution obtained after oxidation with BAHA solution and blue line, reduction with excess hydrazine hydrate solution.
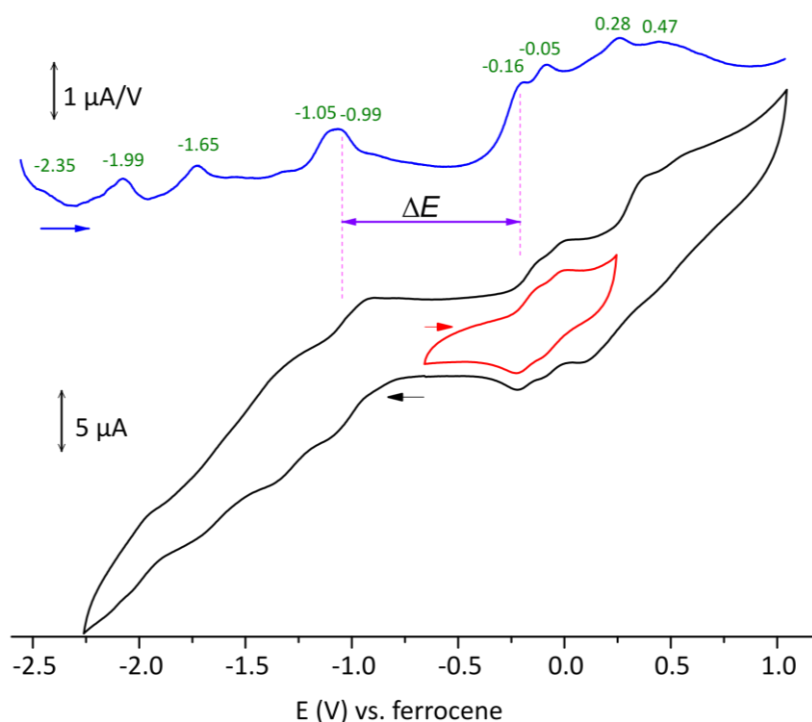
Figure S6. Differential pulse voltammogram (blue) and cyclic voltammogram (black and red) for compound **8** in different potential setup (dichloromethane solvent, [Bu$_4$N]PF$_6$ as supporting electrolyte; glassy carbon, Pt rod, and Ag/AgCl as a working, counter, and reference electrode, respectively, 50 mV/s.
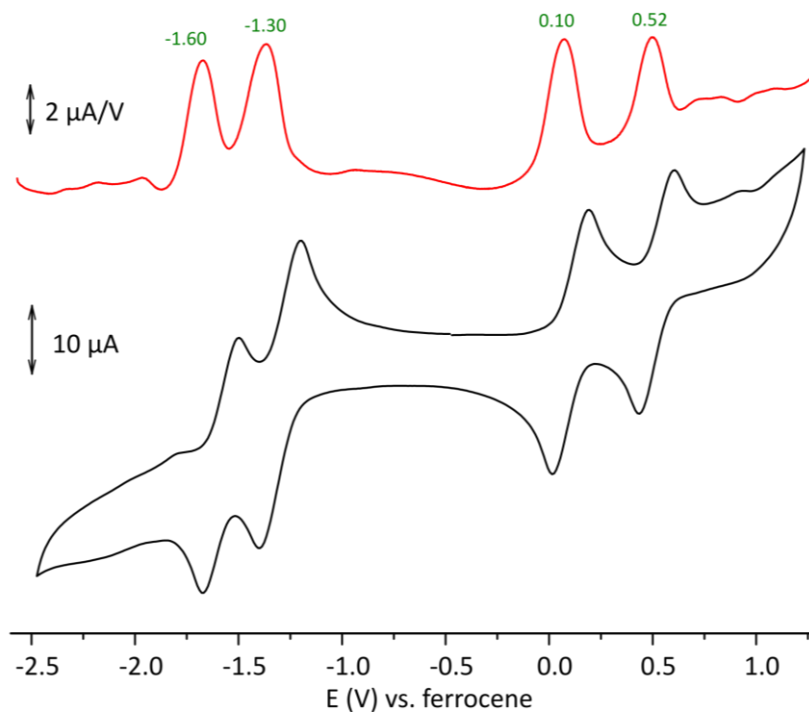
Figure S7. Differential pulse voltammogram and cyclic voltammogram for compound **9** (dichloromethane, [Bu$_4$N]PF$_6$, glassy-carbon electrode, 100 mV/s).
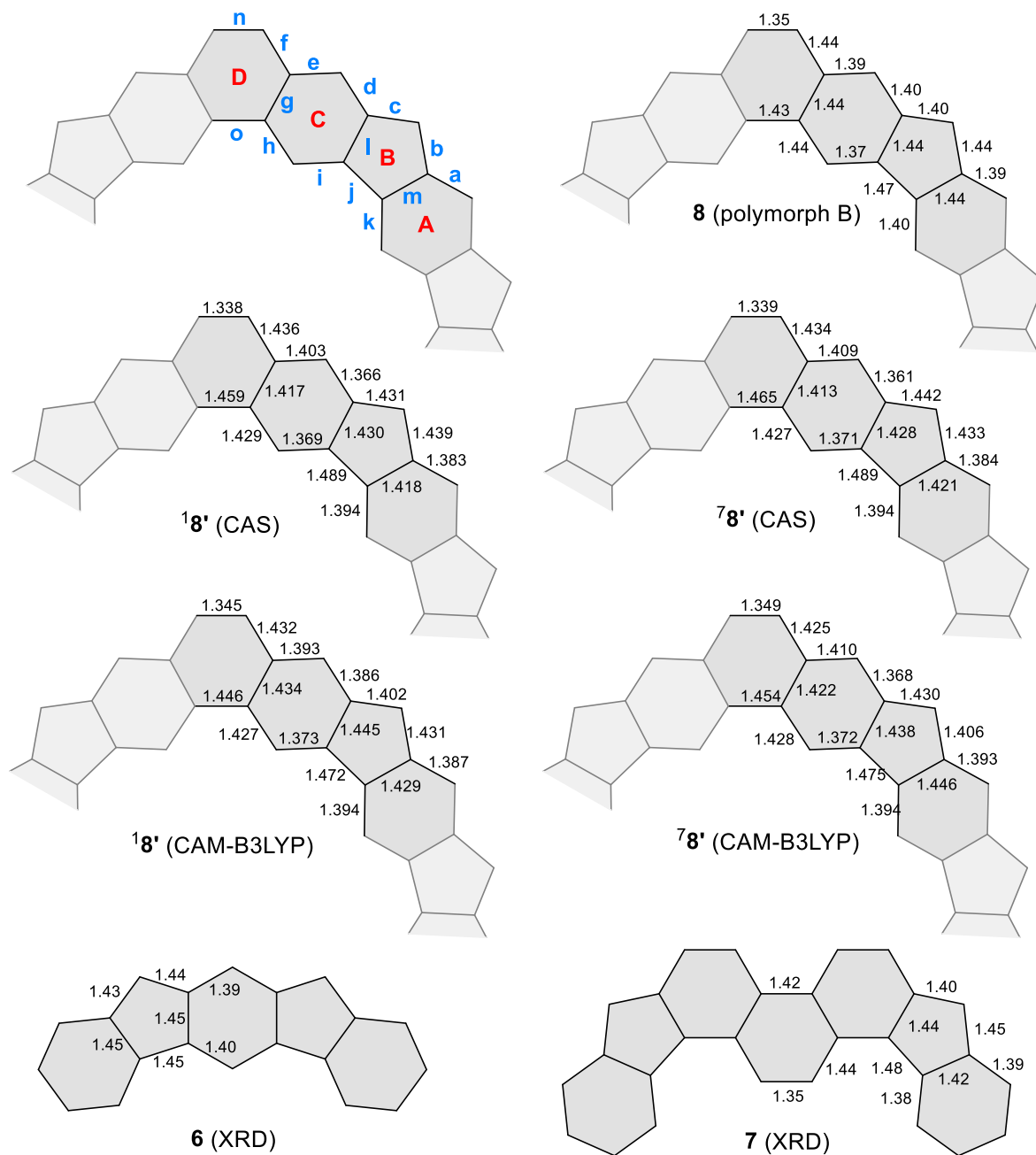
Figure S8. Structure, labeling and bond distances for **8** (polymorph B, symmetry averaged) and **8'** (singlet and septet, CAM, and CAS levels of theory). Selected average distances for published XRD structures of **6** and **7** are given for comparison.
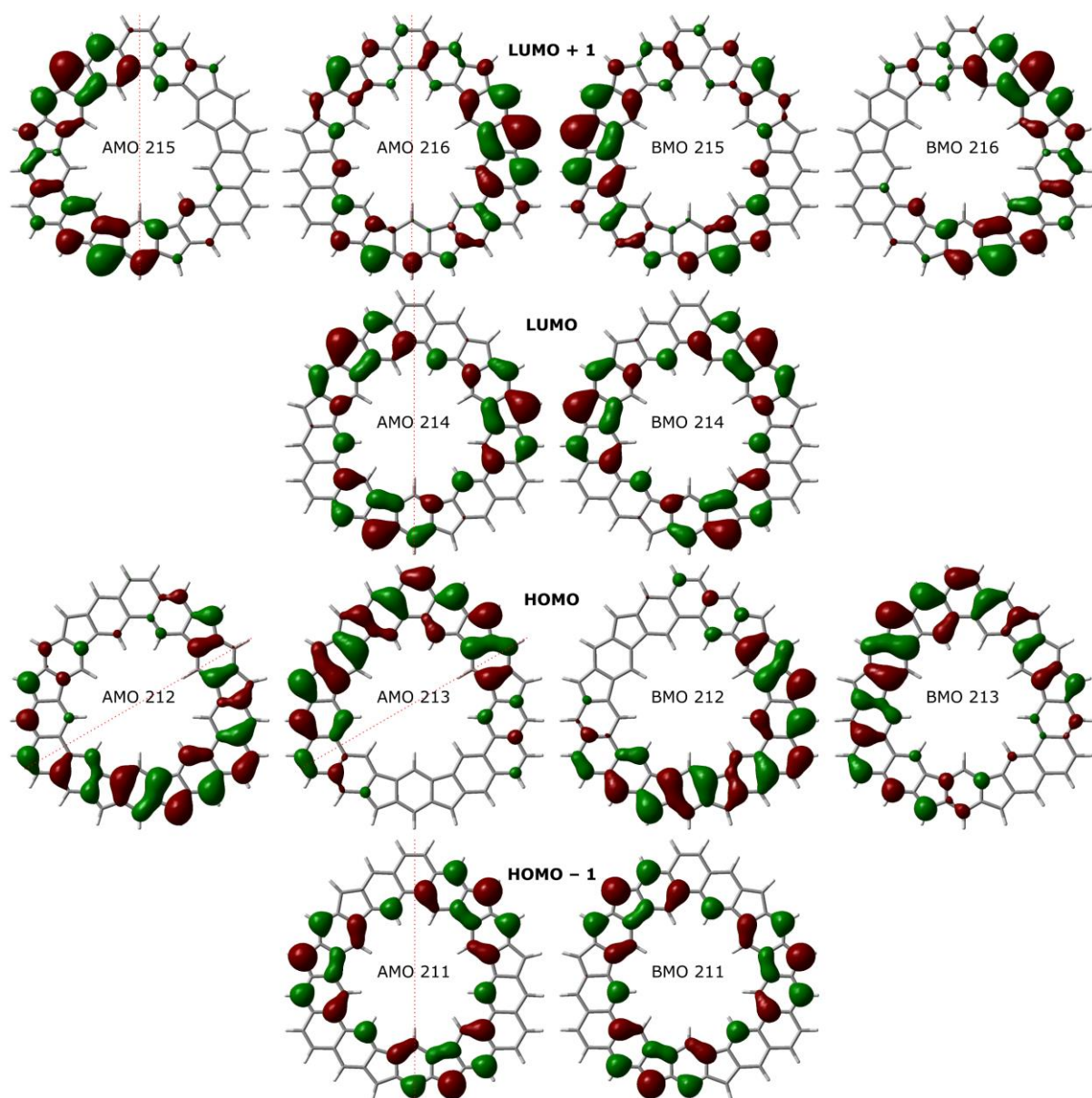
Figure S9. Kohn–Sham α and β molecular orbitals (AMO and BMO, respectively) for ¹**8'** (0.02 a.u. isosurfaces, UCAM-B3LYP/6-31G(d,p)). AMO and BMO wavefunctions are related by mirror planes indicated with dotted lines.
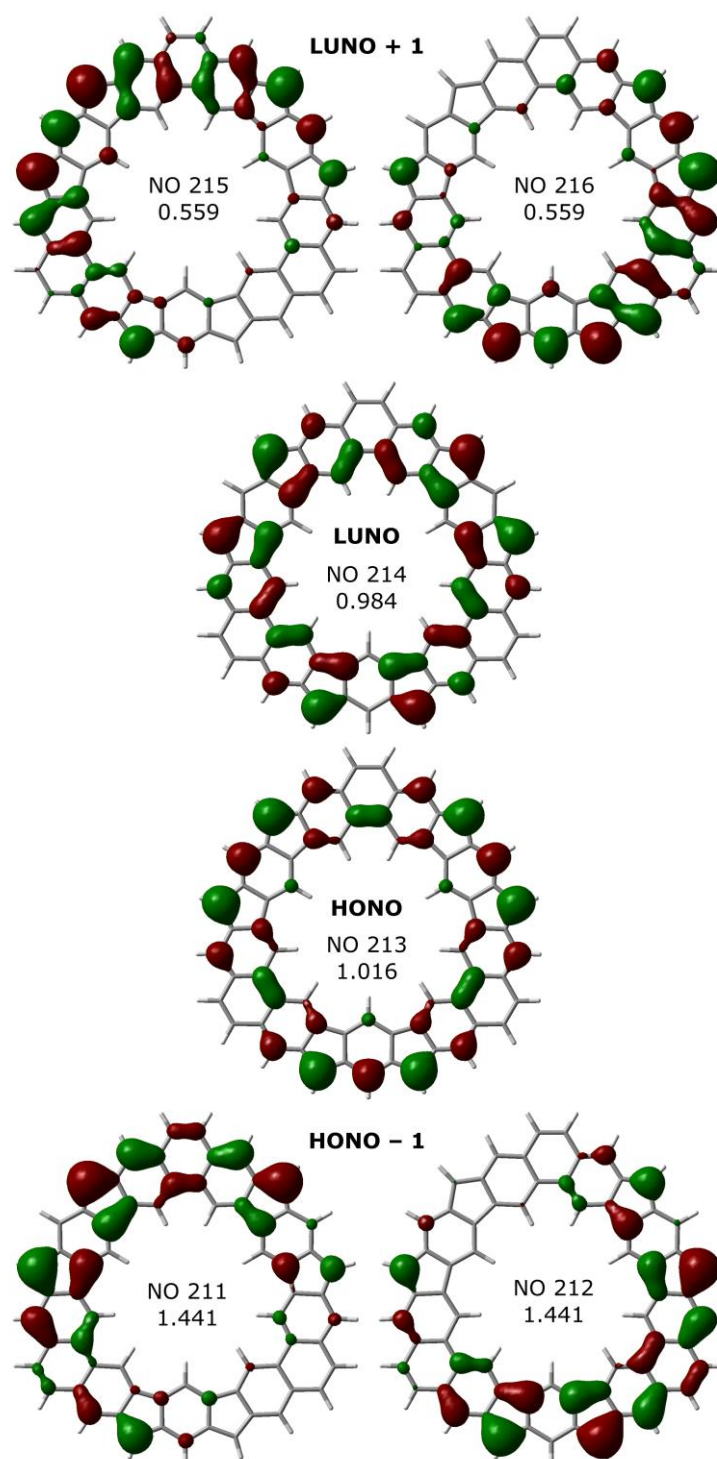
Figure S10. Natural orbitals and their occupation numbers for [1]**8'** (0.02 a.u. isosurfaces, UCAM-B3LYP/6-31G(d,p) density).
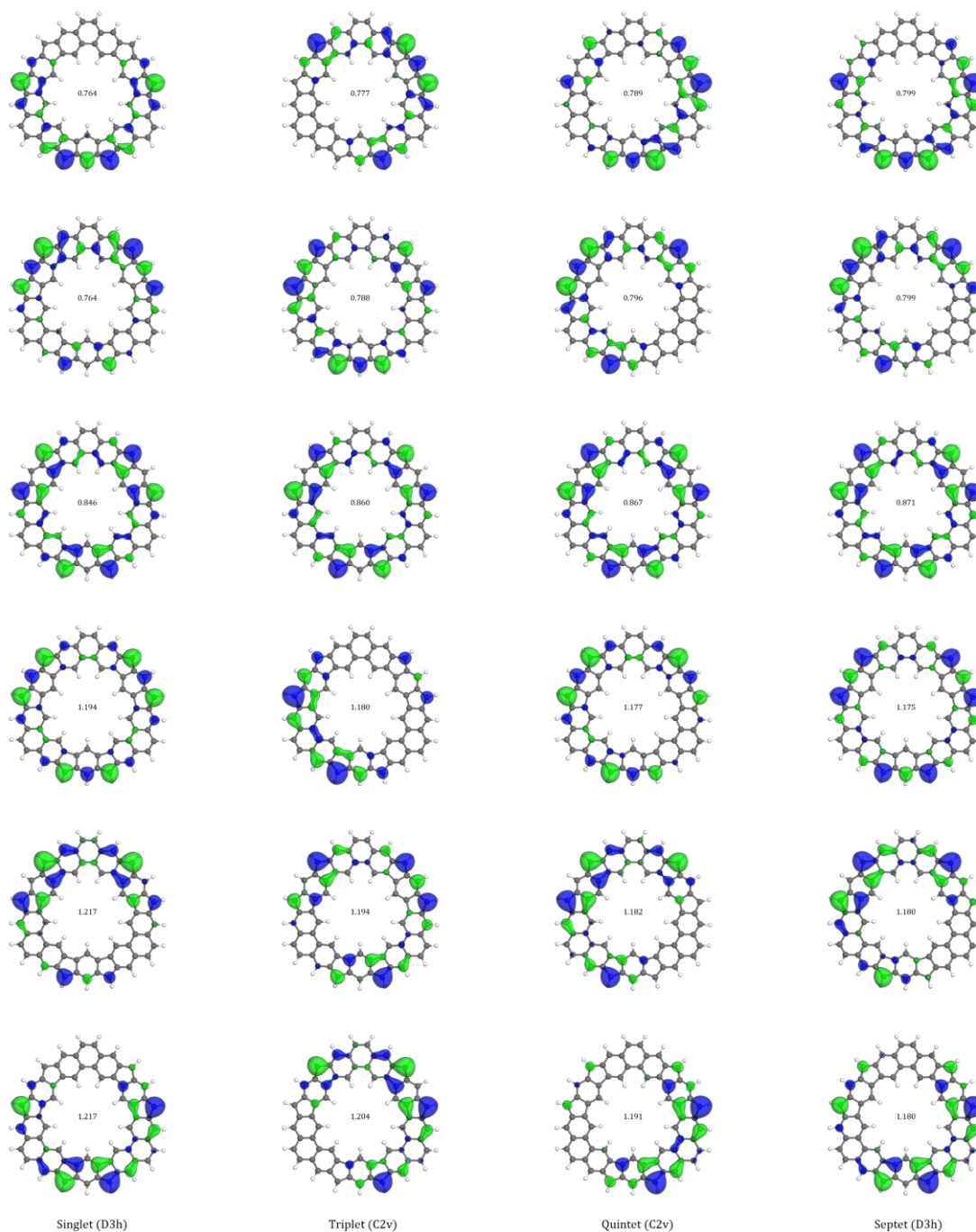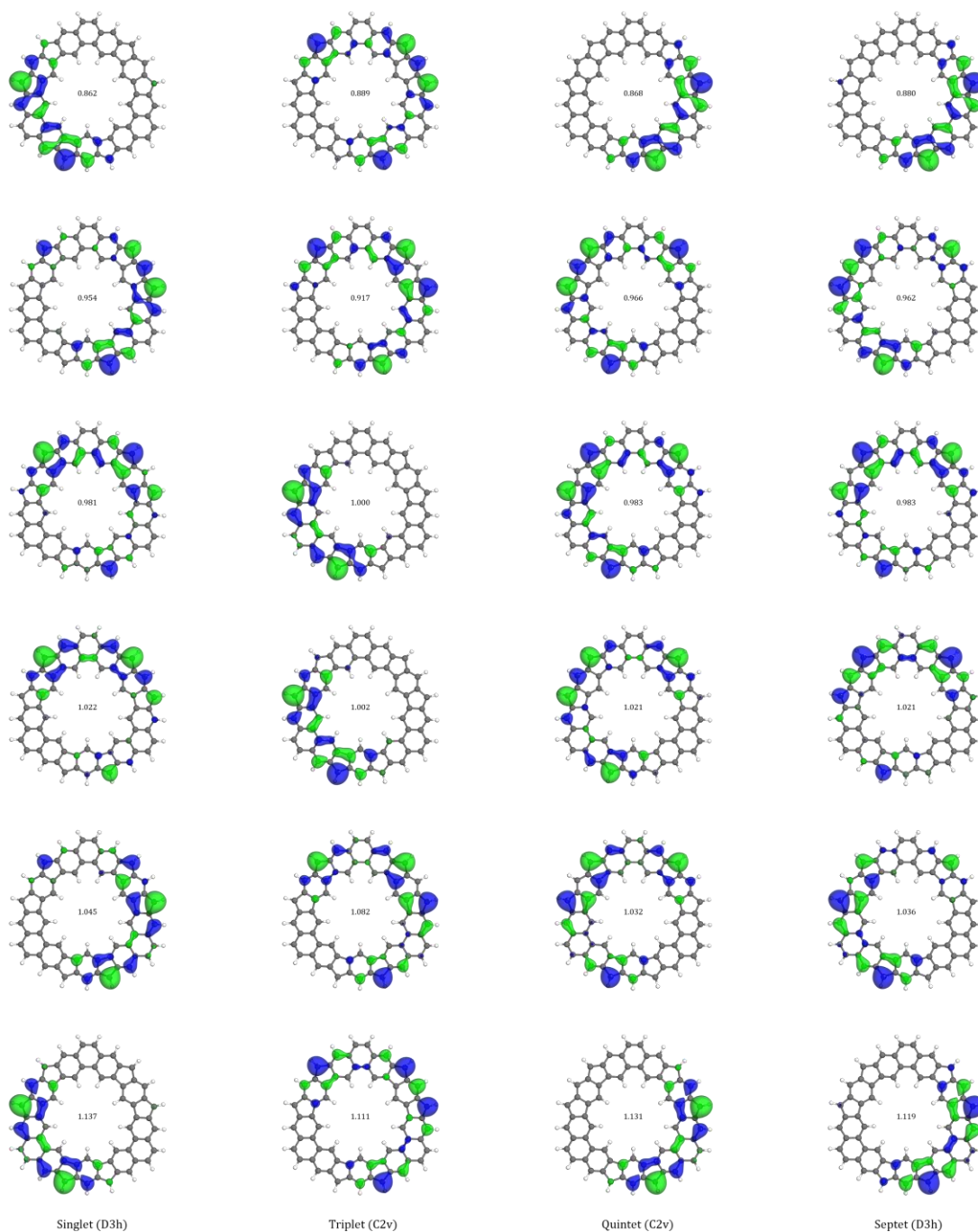
Figure S11. Natural orbitals for the RAS(6,6)-SF/cc-pVDZ ground state (S_1) at CASSCF(6,6)/CC-PVDZ geometries optimized for the singlet (^{1}**8'**), triplet (^{3}**8'**), quintet (^{5}**8'**), and septet (^{7}**8'**) configurations.
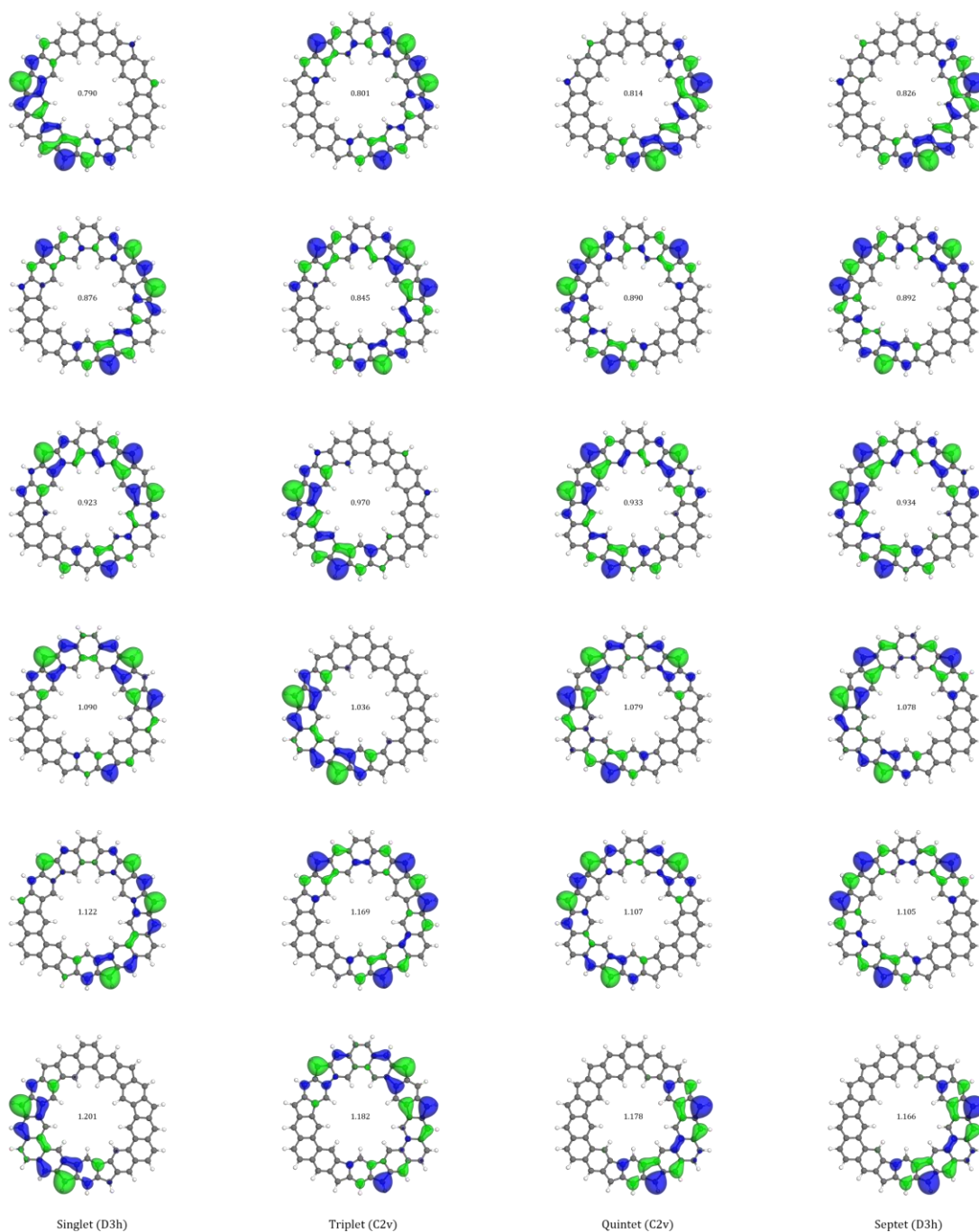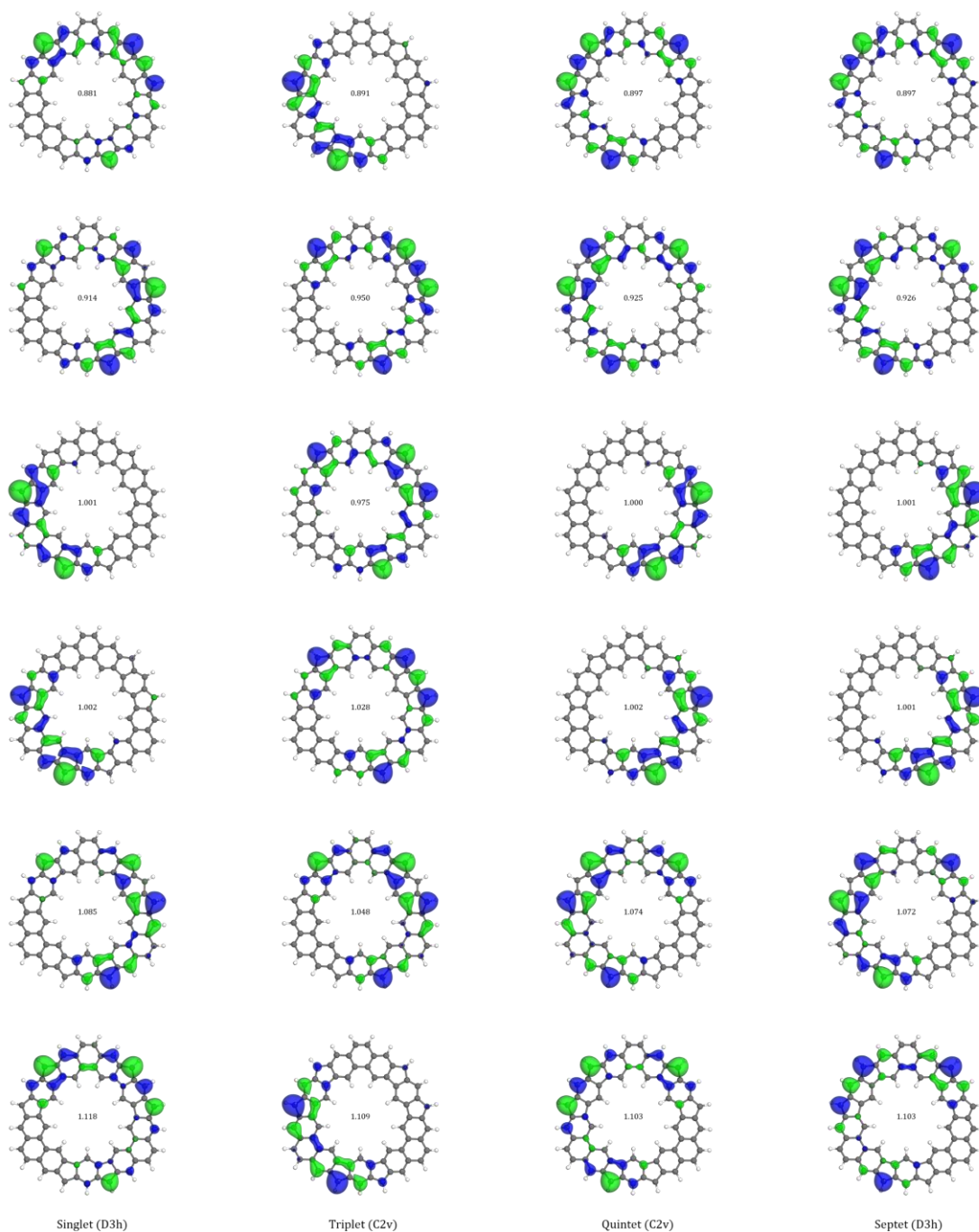
Figure S12. Natural orbitals for the RAS(6,6)-SF/cc-pVDZ T_1 excited state at CASSCF(6,6)/CC-PVDZ geometries optimized for the singlet (^{1}**8'**), triplet (^{3}**8'**), quintet (^{5}**8'**), and septet (^{7}**8'**) configurations.
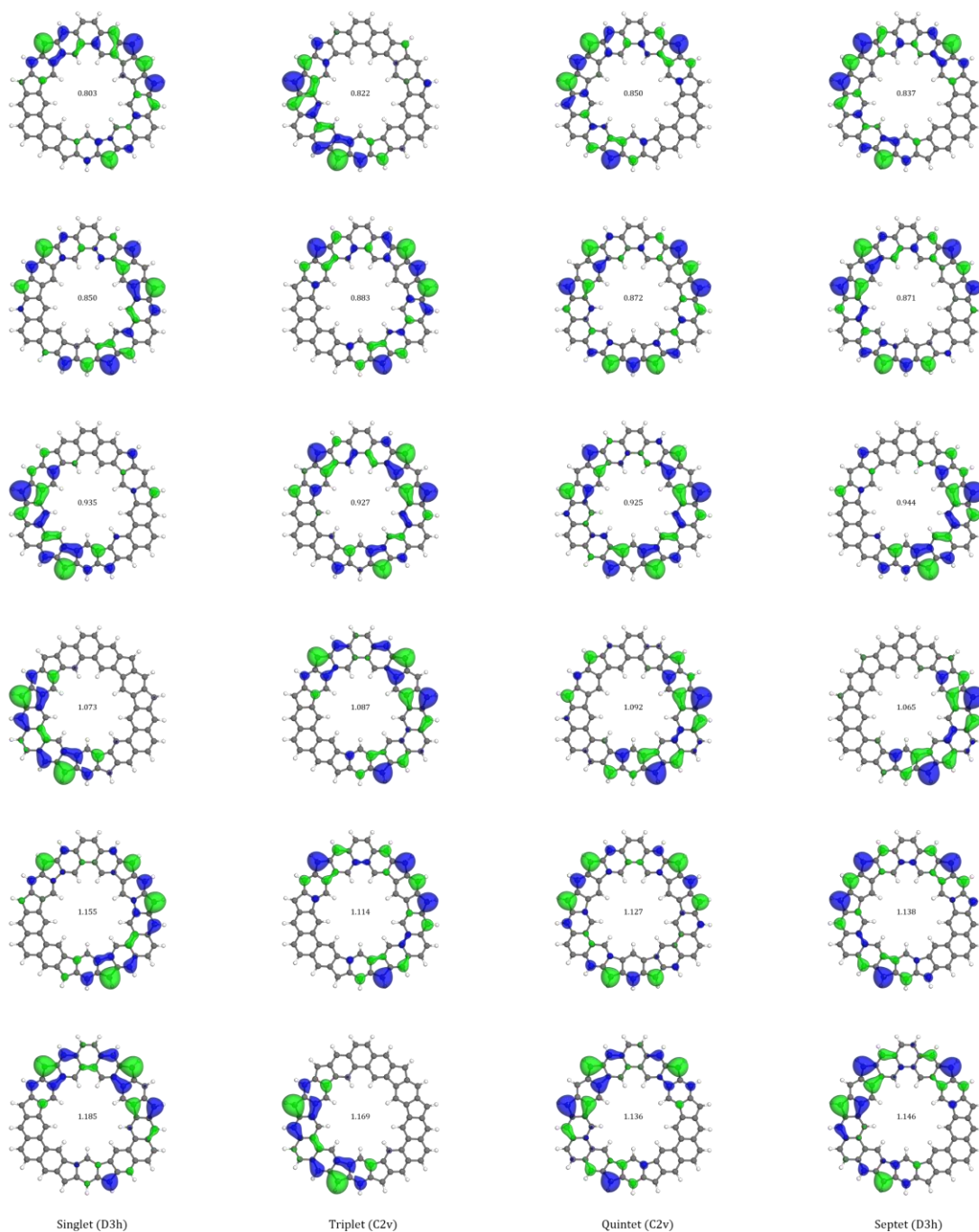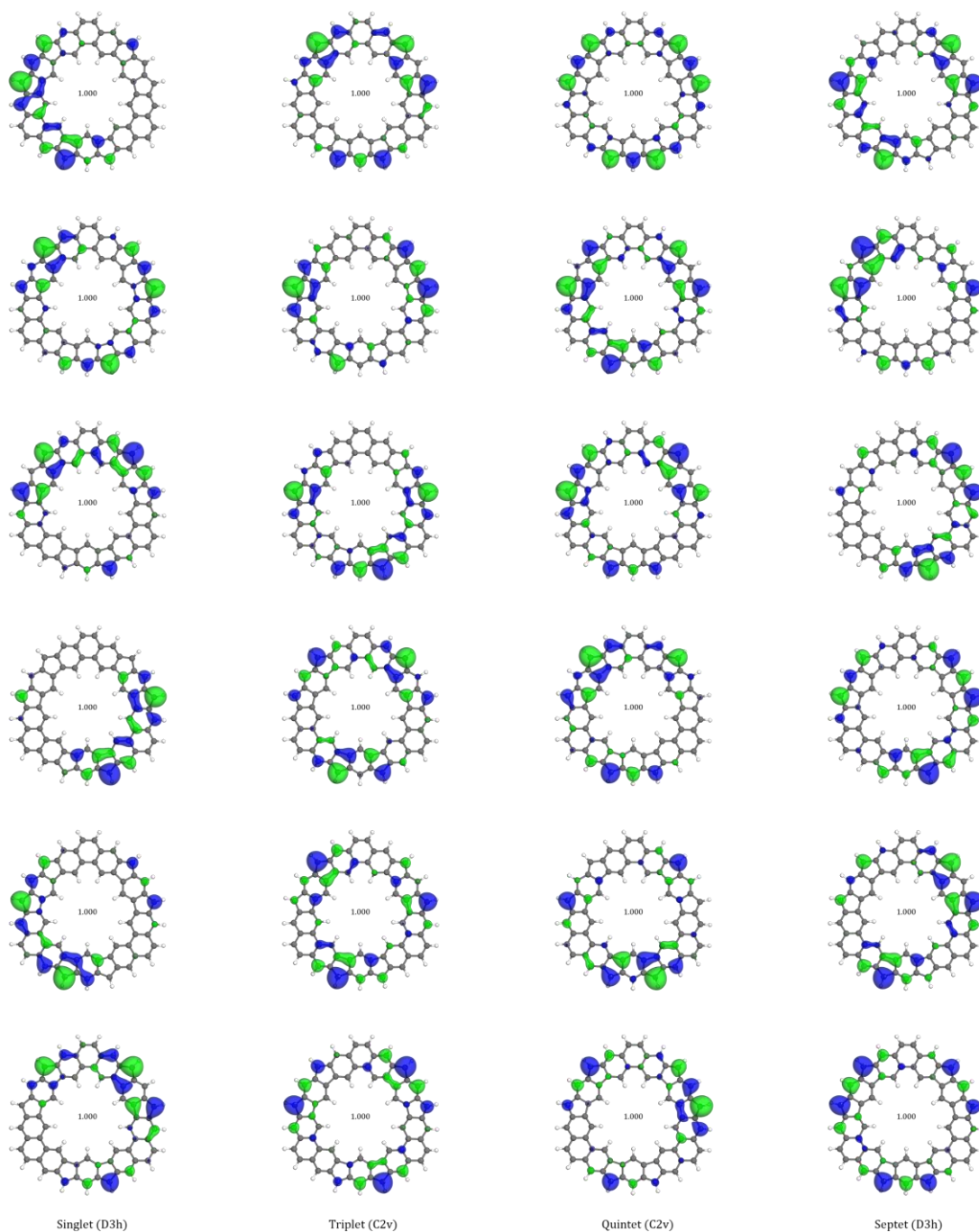
Figure S13. Natural orbitals for the RAS(6,6)-SF/cc-pVDZ T_2 excited state at CASSCF(6,6)/CC-PVDZ geometries optimized for the singlet (^{1}**8'**), triplet (^{3}**8'**), quintet (^{5}**8'**), and septet (^{7}**8'**) configurations.
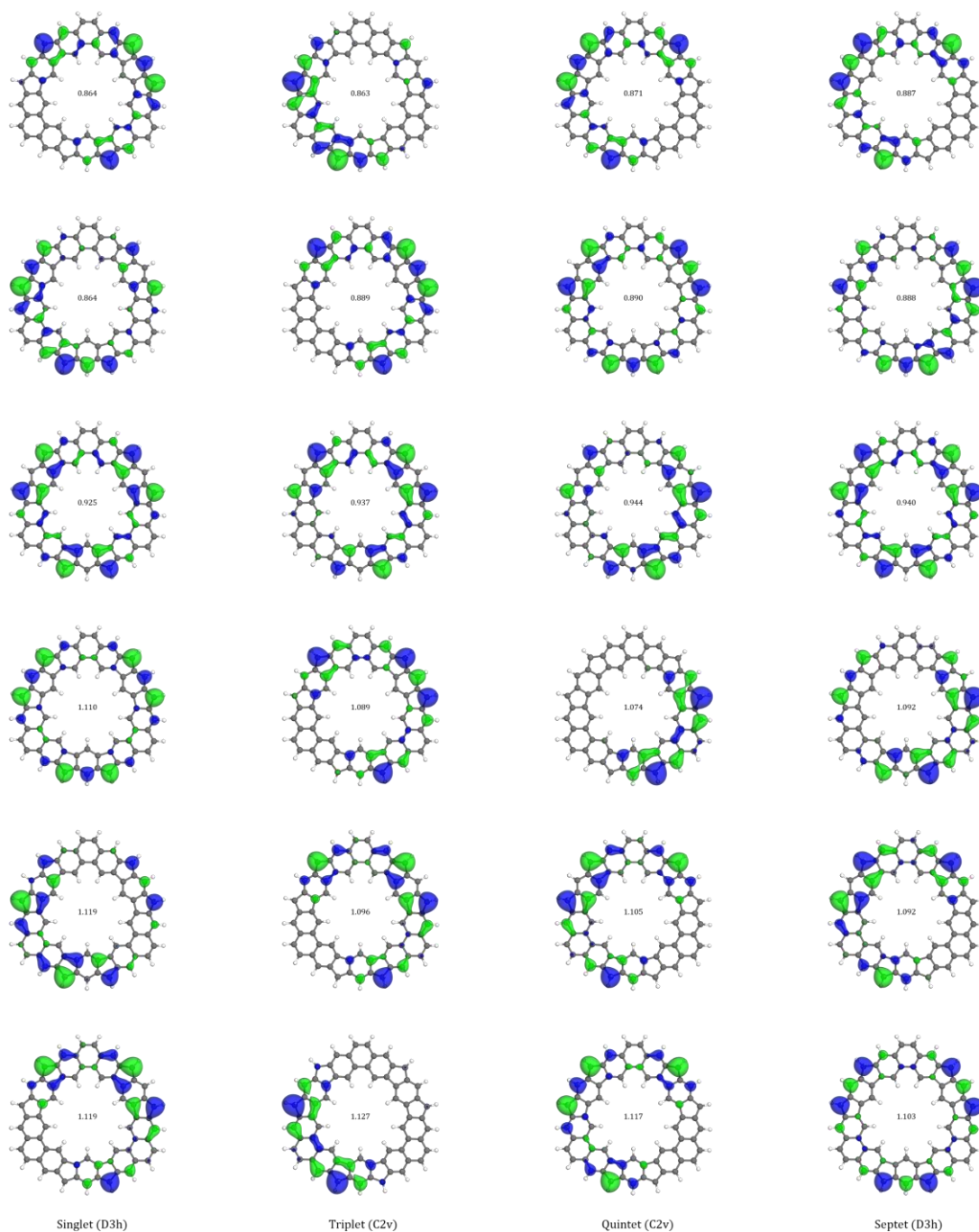
Figure S14. Natural orbitals for the RAS(6,6)-SF/cc-pVDZ T$_3$ excited state at CASSCF(6,6)/CC-PVDZ geometries optimized for the singlet (^{1}**8'**), triplet (^{3}**8'**), quintet (^{5}**8'**), and septet (^{7}**8'**) configurations.

Figure S15. Natural orbitals for the RAS(6,6)-SF/cc-pVDZ Qn_1 excited state at CASSCF(6,6)/CC-PVDZ geometries optimized for the singlet (^{1}**8'**), triplet (^{3}**8'**), quintet (^{5}**8'**), and septet (^{7}**8'**) configurations.

Figure S16. Natural orbitals for the RAS(6,6)-SF/cc-pVDZ Qn_2 excited state at CASSCF(6,6)/CC-PVDZ geometries optimized for the singlet (^{1}**8'**), triplet (^{3}**8'**), quintet (^{5}**8'**), and septet (^{7}**8'**) configurations.

Singlet (D3h) Triplet (C2v) Quintet (C2v) Septet (D3h)

Figure S17. Natural orbitals for the RAS(6,6)-SF/cc-pVDZ Spt$_1$ excited state at CASSCF(6,6)/CC-PVDZ geometries optimized for the singlet (^{1}**8'**), triplet (^{3}**8'**), quintet (^{5}**8'**), and septet (^{7}**8'**) configurations.
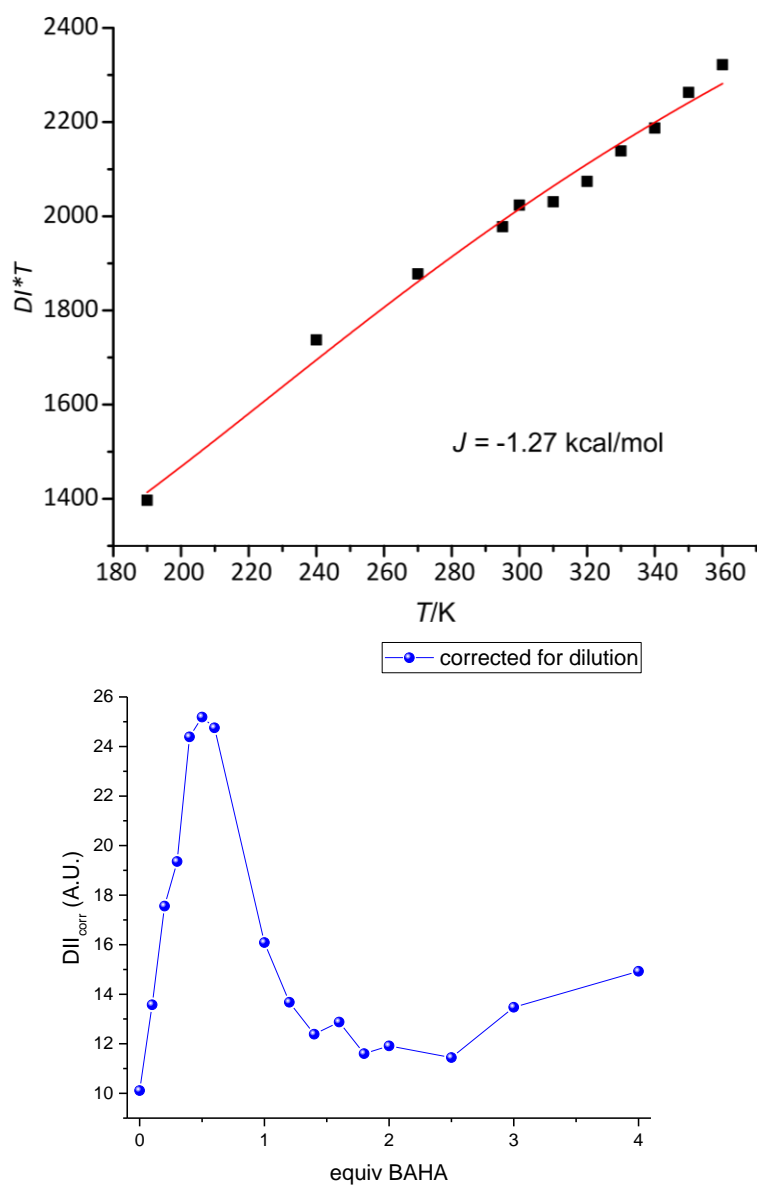
Figure S18. Top: Temperature dependence of the product of temperature and doubly integrated ESR signal intensity. The red line represents the best fit of data points to the Bleaney-Bowers equation with exchange integral –1.27 kcal/mol. Bottom: Changes of doubly integrated ESR signal intensity (corrected for dilution) during titration of **8** with BAHA (CDCl3/MeCN-d_3 mixture).
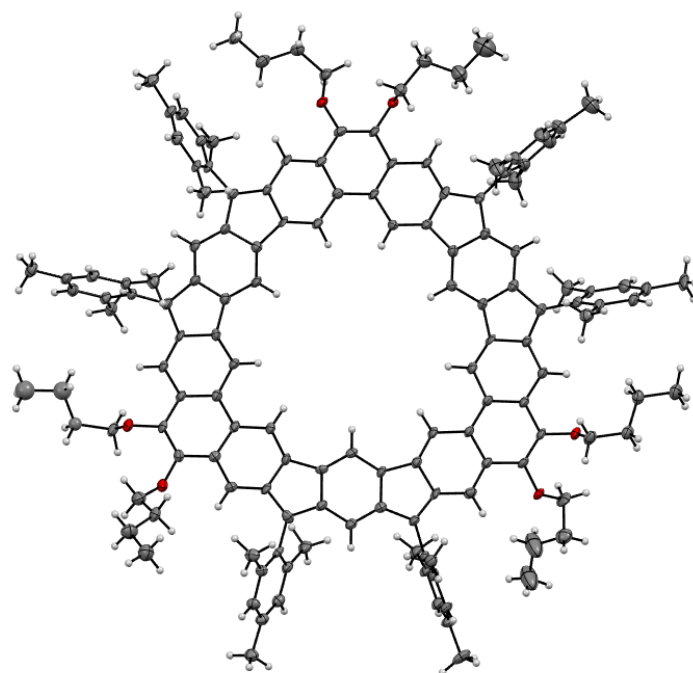
Figure S19. Crystal structure for **8** (polymorph A). Disorder in OBu groups and solvent molecules were removed for clarity.
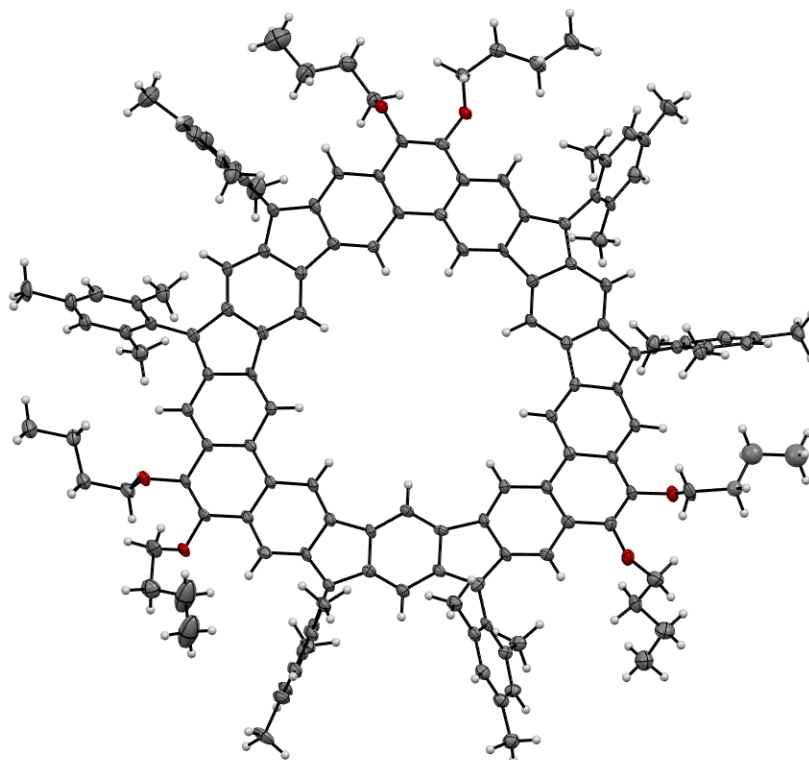
Figure S20. Crystal structure for **8** (polymorph B). Disorder in OBu groups and solvent molecules were removed for clarity.

Additional Tables

Table S2. Comparison of selected chemical shifts for compounds **5–9**.

Species	Reference	Chemical shift [ppm]			Ring current
		m-Mes	*o*-Mes	*p*-Mes	
5²⁺ (chloroform-*d*, 300 K)	1	8.15	2.77	3.18	diatropic
7 (CDCl₃, 220 K)	19	7.00	2.11	2.35	none
9 (DCM-*d*₂, 190 K)	this work	6.98	2.06	2.31	none
8 (DCFM-*d*, 160 K)	this work	6.72	1.90	2.14	moderately paratropic
5 (toluene-*d*₈ + chloroform-*d*, 200 K)	1	6.15	1.98	1.74	paratropic

Table S3. DFT calculations for **6'**, **8'** and **9'**.

Symbol	Name [a]	Mult [b]	SCF *E* [c]	ZPV [d]	Lowest freq. [e]	G [f]	ΔSCFrel [g]	<*S*²> [h]
			a.u.	a.u.	cm⁻¹	a.u.	kcal/mol	a.a.
¹**6'**	Tobe_0_1	1	-768.931868	0.252820	53.56	-768.718866	0.63	0.519
³**6'**	Tobe_0_3	3	-768.932873	0.252962	54.30	-768.720789	0.00	2.006
¹**8'**	b3HH_0_1	1	-2531.843875	0.736004	7.79	-2531.179820	0.00	10.149
³**8'**	b3HH_0_3	3	-2531.841257	0.736223	7.66	-2531.177992	1.64	5.376
⁵**8'**	b3HH_0_5	5	-2531.842613	0.736432	7.04	-2531.179735	0.79	6.388
⁷**8'**	b3HH_0_7	7	-2531.843722	0.736671	6.86	-2531.181070	0.10	12.028
¹**9'**	MM_0_1	1	-1076.071158	0.347842	35.68	-1075.770105	0.00	1.042
³**9'**	MM_0_3	3	-1076.067350	0.347867	35.26	-1075.767300	2.39	2.006

[a] Geometry available as a separate xyz file. [b] Multiplicity. [c] SCF energy. [d] Zero-point vibrational energy. [e] Lowest vibrational frequency. [f] Gibbs free energy. [g] Relative SCF energy. [h] After annihilation of the first spin contaminant

Table S4. Crystal data and structure refinement for **8** (polymorph A).

Identification code	bb211
Empirical formula	$C_{179}H_{178}O_6$
Formula weight	2425.20
Temperature	100(2) K
Wavelength	1.54184 Å
Crystal system	Orthorhombic
Space group	$P2_12_12_1$
Unit cell dimensions	a = 41.834(11) Å $\alpha = 90°$.
	b = 20.726(4) Å $\beta = 90°$.
	c = 15.823(6) Å $\gamma = 90°$.
Volume	13719(7) Å^3
Z	4
Density (calculated)	1.174 Mg/m^3
Absorption coefficient	0.526 mm^{-1}
F(000)	5200
Crystal size	0.210 x 0.040 x 0.030 mm^3
Theta range for data collection	2.112 to 73.218°.
Index ranges	-51<=h<=50, -16<=k<=25, -19<=l<=19
Reflections collected	60431
Independent reflections	24253 [R(int) = 0.0668]
Completeness to theta = 67.000°	99.5 %
Absorption correction	Semi-empirical from equivalents
Max. and min. transmission	1.00000 and 0.76658
Refinement method	Full-matrix least-squares on F^2
Data / restraints / parameters	24253 / 25 / 1467
Goodness-of-fit on F^2	1.108
Final R indices [I>2sigma(I)]	R1 = 0.1143, wR2 = 0.3027
R indices (all data)	R1 = 0.1746, wR2 = 0.3463
Absolute structure parameter	0.0(2)
Extinction coefficient	n/a
Largest diff. peak and hole	0.479 and -0.569 e. Å^{-3}

Table S5. Crystal data and structure refinement for **8** (polymorph B).

Identification code	bb211ba
Empirical formula	$C_{165}H_{162}O_6$
Formula weight	2240.94
Temperature	100(2) K
Wavelength	1.54184 Å
Crystal system	Orthorhombic
Space group	$P2_12_12_1$
Unit cell dimensions	a = 15.664(3) Å $\quad$ α = 90°.
	b = 22.270(6) Å $\quad$ β = 90°.
	c = 37.156(13) Å $\quad$ γ = 90°.
Volume	12961(6) $Å^3$
Z	4
Density (calculated)	1.148 Mg/m^3
Absorption coefficient	0.517 mm^{-1}
F(000)	4800
Crystal size	0.550 x 0.040 x 0.020 mm^3
Theta range for data collection	2.313 to 66.999°.
Index ranges	-12<=h<=18, -26<=k<=26, -43<=l<=44
Reflections collected	83290
Independent reflections	22886 [R(int) = 0.1005]
Completeness to theta = 67.000°	99.7 %
Absorption correction	Analytical
Max. and min. transmission	0.988 and 0.804
Refinement method	Full-matrix least-squares on F^2
Data / restraints / parameters	22886 / 8 / 1525
Goodness-of-fit on F^2	1.082
Final R indices [I>2sigma(I)]	R1 = 0.0923, wR2 = 0.2083
R indices (all data)	R1 = 0.1598, wR2 = 0.2462
Absolute structure parameter	-0.2(2)
Extinction coefficient	n/a
Largest diff. peak and hole	0.492 and -0.331 e. $Å^{-3}$

NMR Spectra
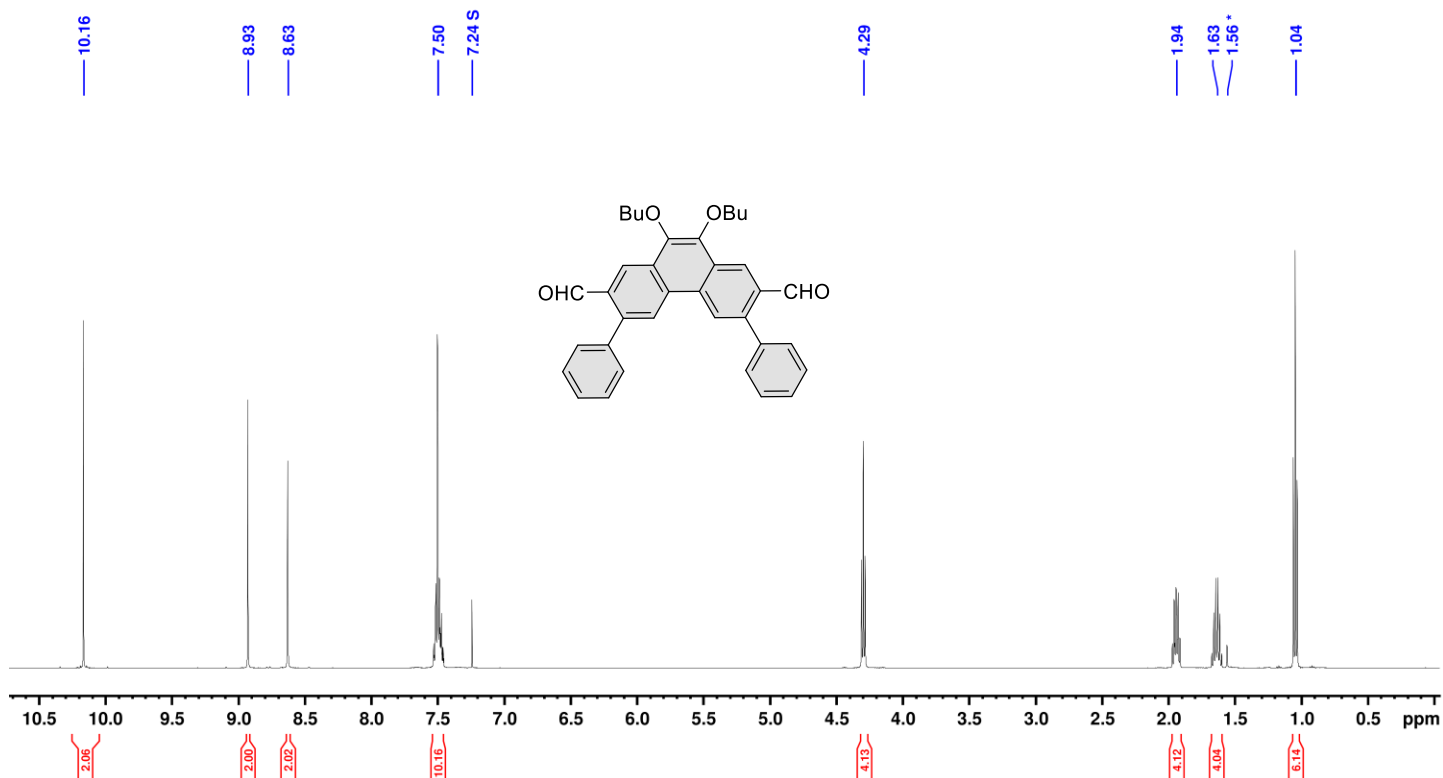
Figure S21. ^{1}H NMR spectrum of **S1** (500 MHz, chloroform-*d*, 300 K).
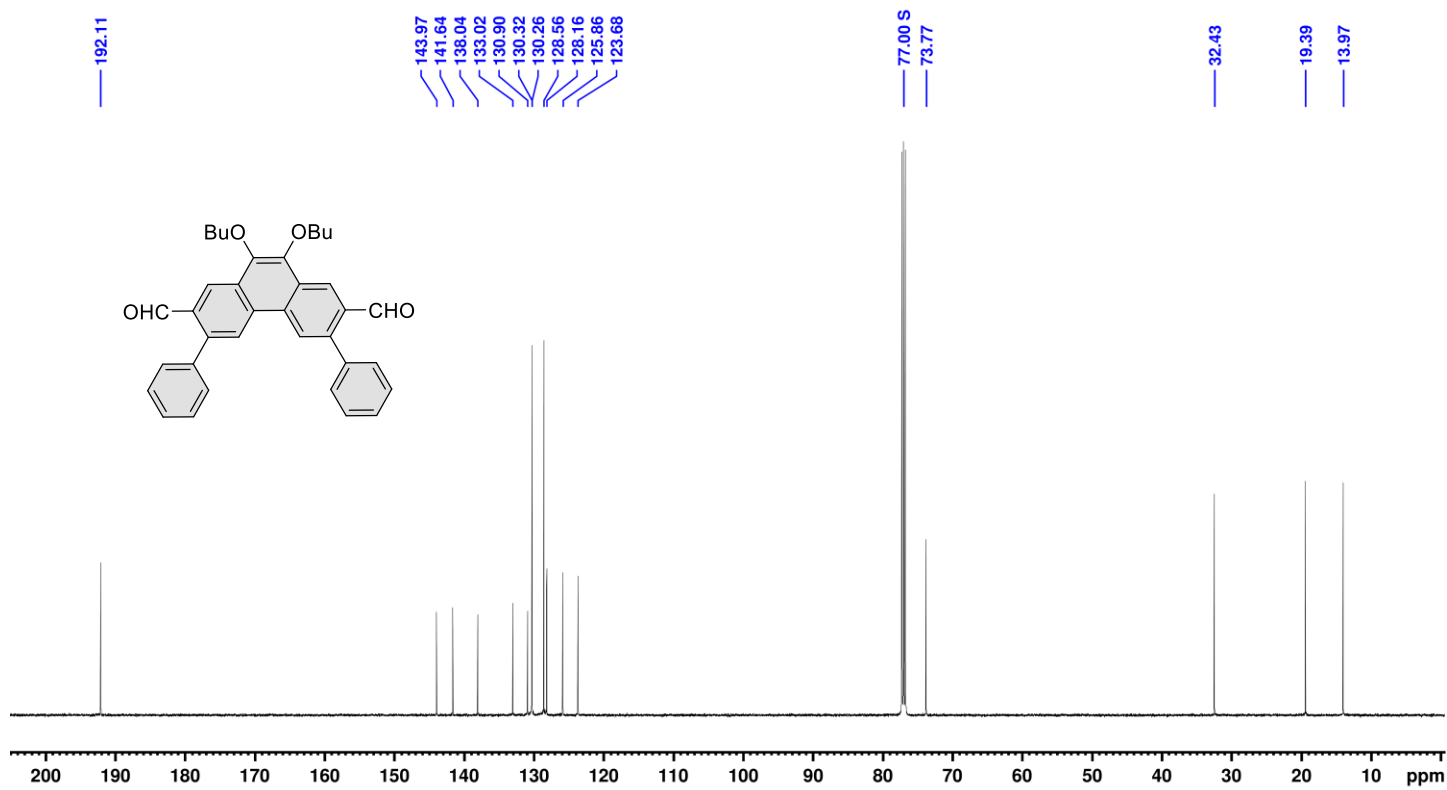
Figure S22. ^{13}C NMR spectrum of **S1** (125 MHz, chloroform-*d*, 300 K).
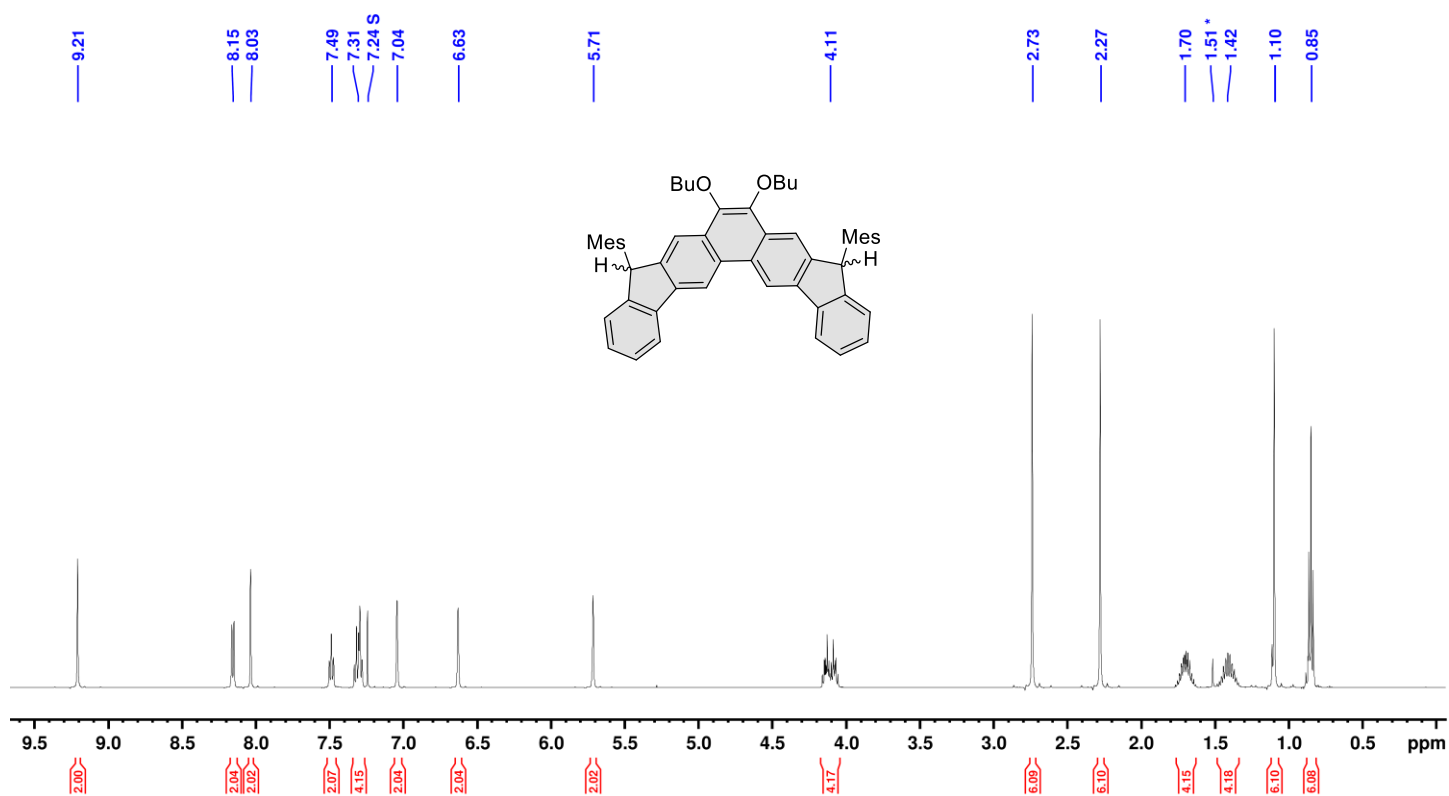
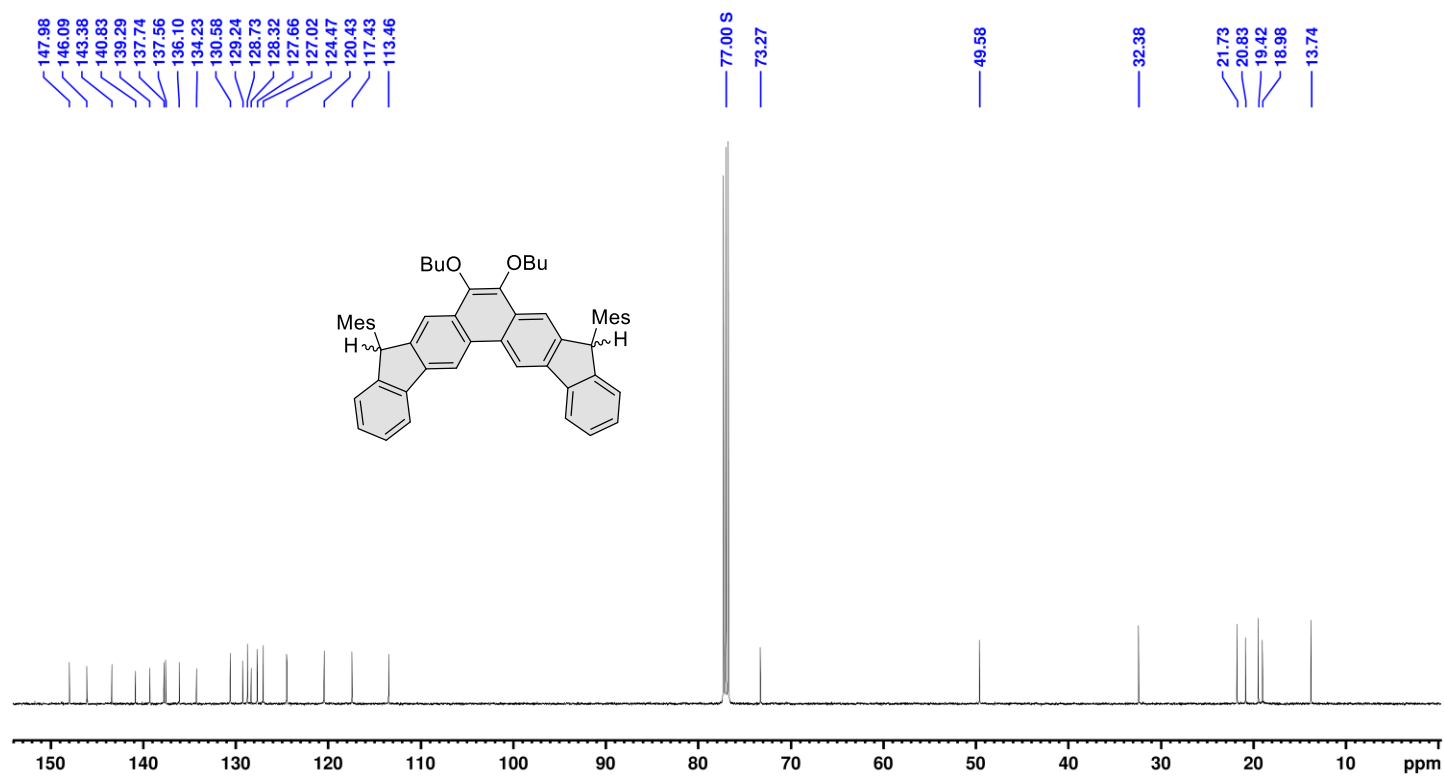**Figure S23.** ^{1}H NMR spectrum of **S2** (500 MHz, chloroform-*d*, 300 K).

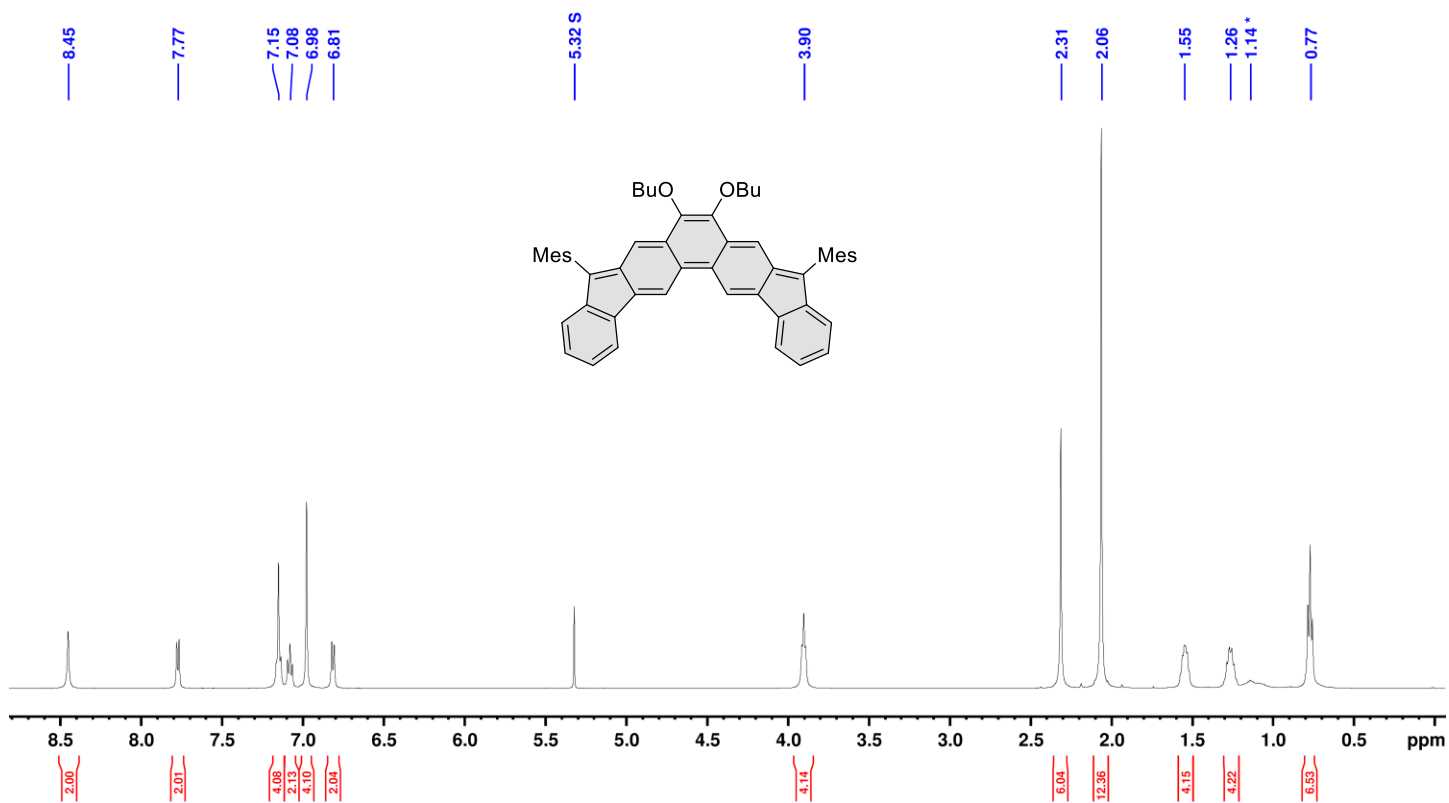**Figure S24.** ^{13}C NMR spectrum of **S2** (125 MHz, chloroform-*d*, 300 K).

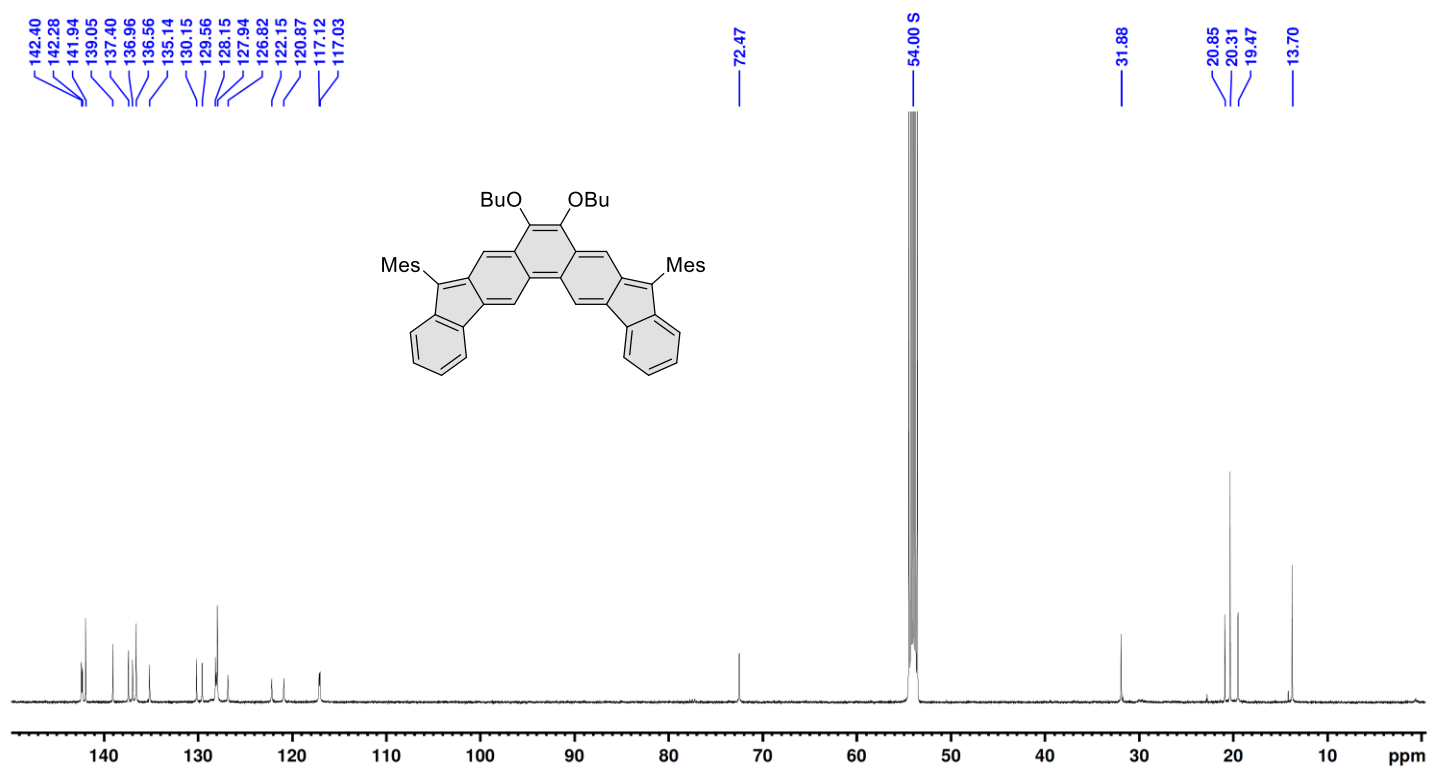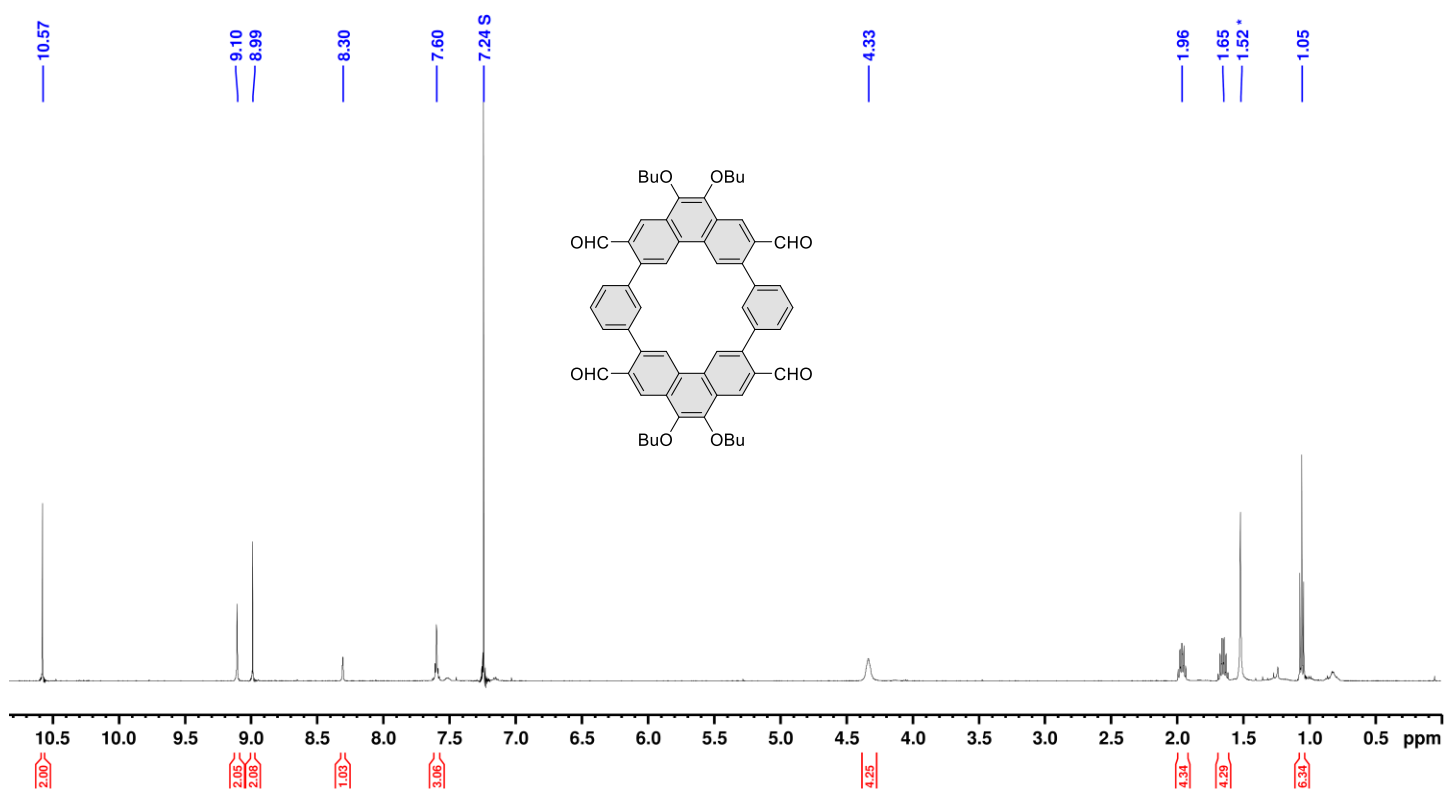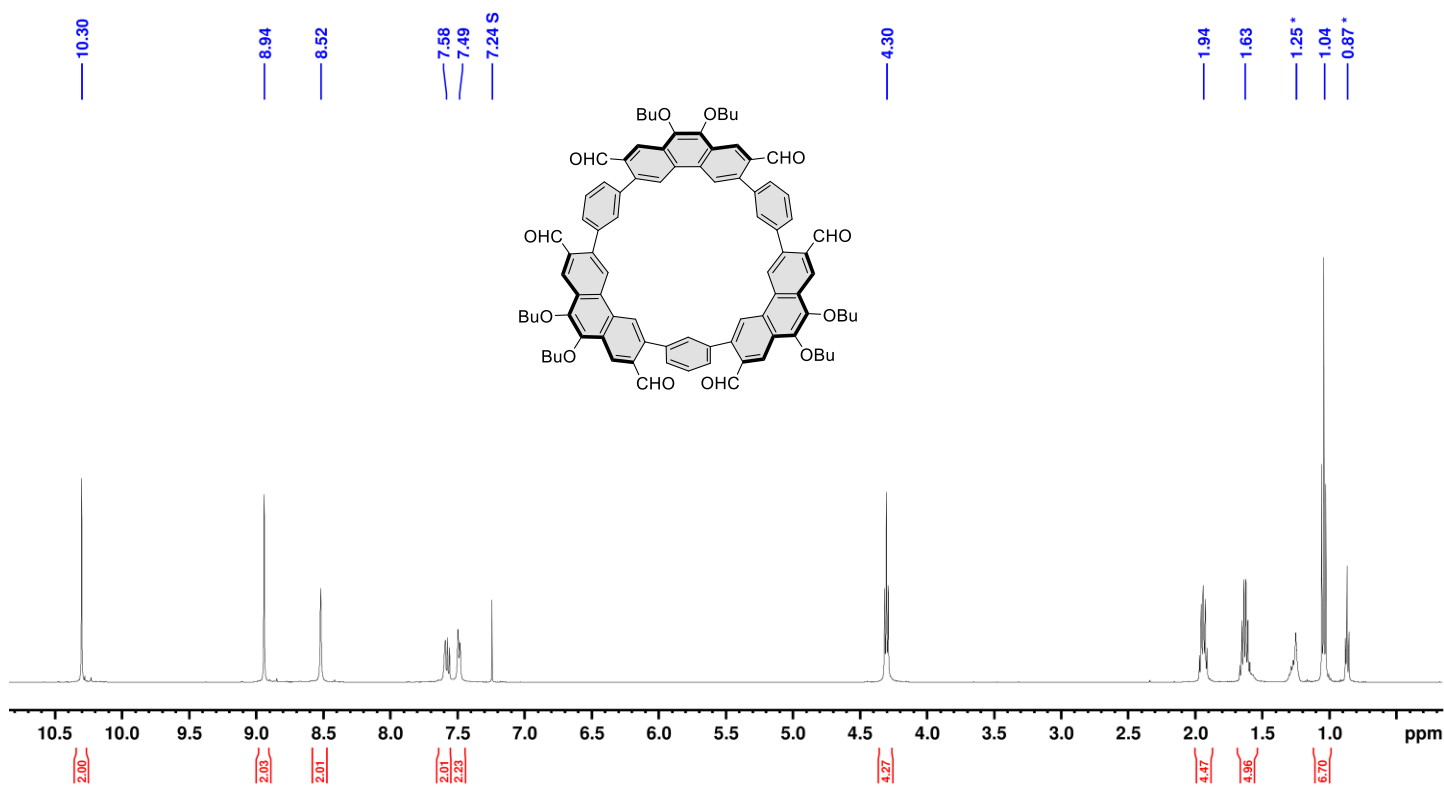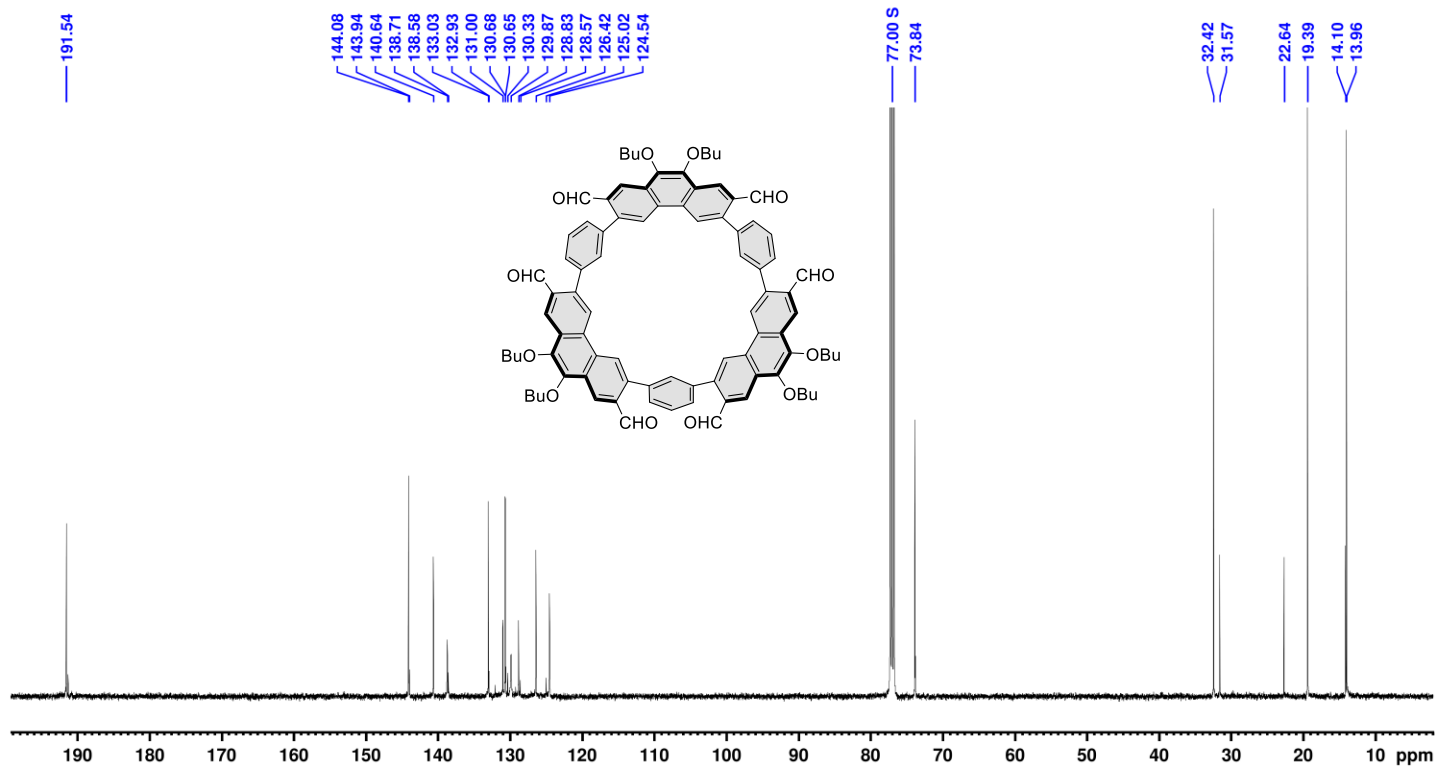**Figure S25.** ^{1}H NMR spectrum of compound **9** (500 MHz, dichloromethane-d_2, 190 K).

Figure S26. ^{13}C NMR spectrum of **9** (125 MHz, dichloromethane-d_2, 190 K).

Figure S27. ^{1}H NMR spectrum of compound **11a** (500 MHz, chloroform-*d*, 300 K).
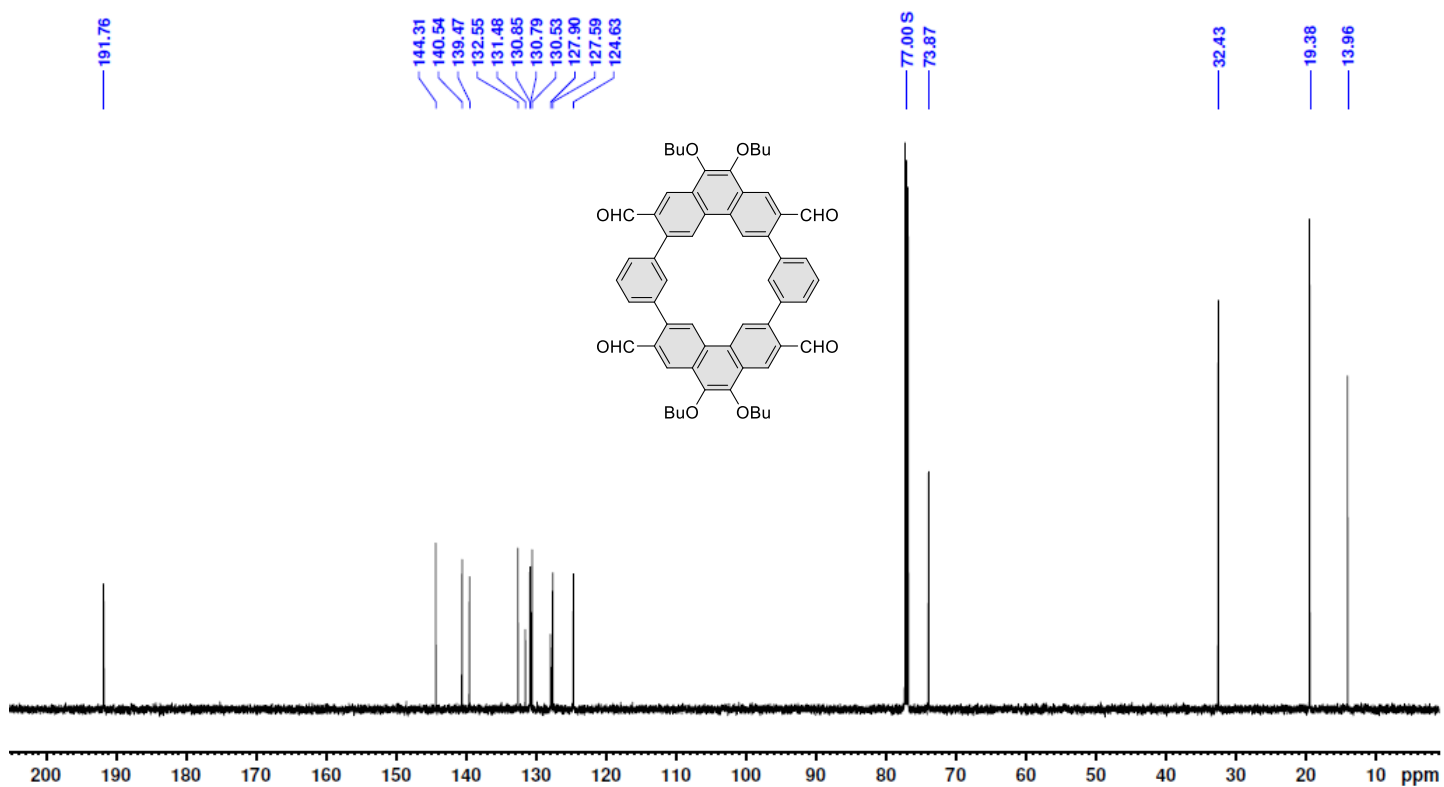
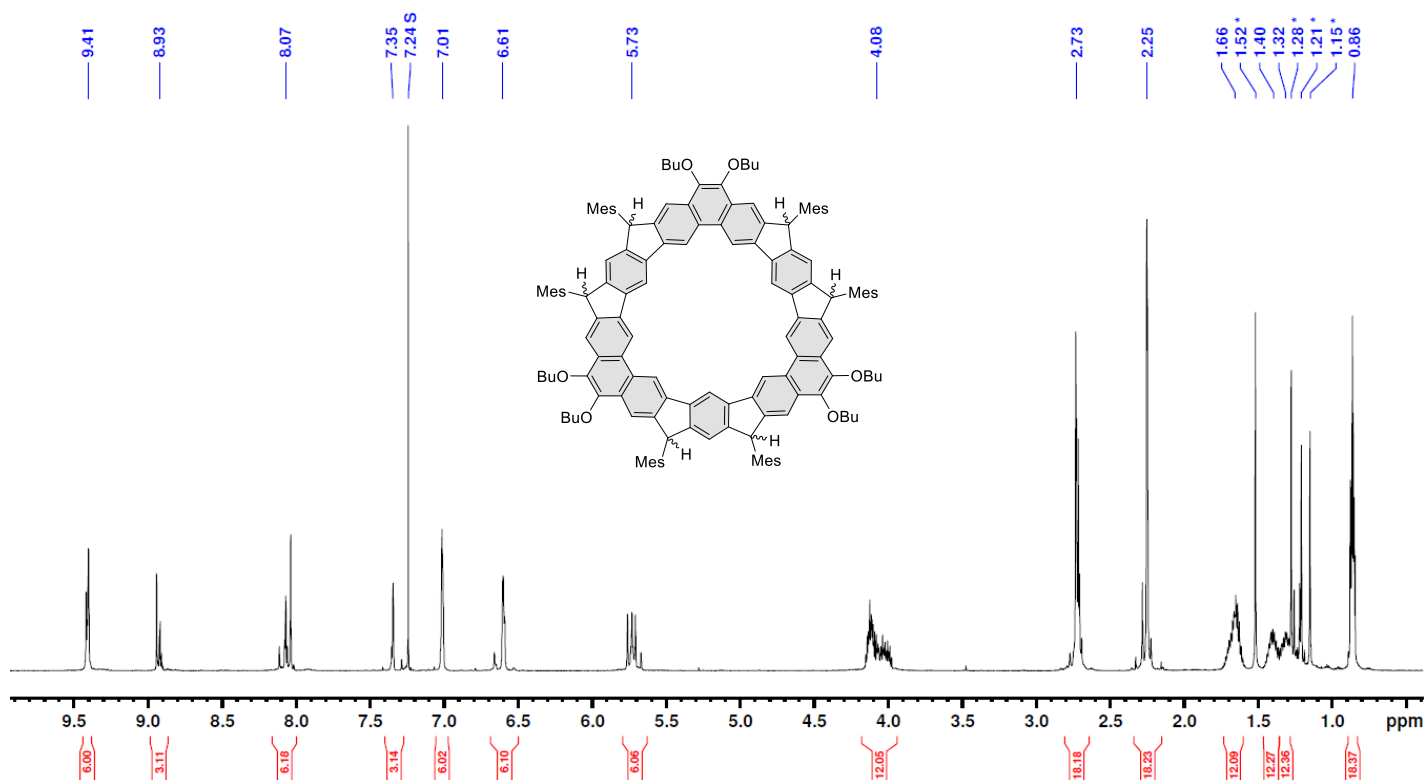**Figure S28.** ^{13}C NMR spectrum of **11a** (151 MHz, chloroform-*d*, 300 K).

Figure S29. ^{1}H NMR spectrum of compound **11b** (500 MHz, chloroform-*d*, 300 K).

Figure S30. ^{13}C NMR spectrum of compound **11b** (125 MHz, chloroform-*d*, 300 K).

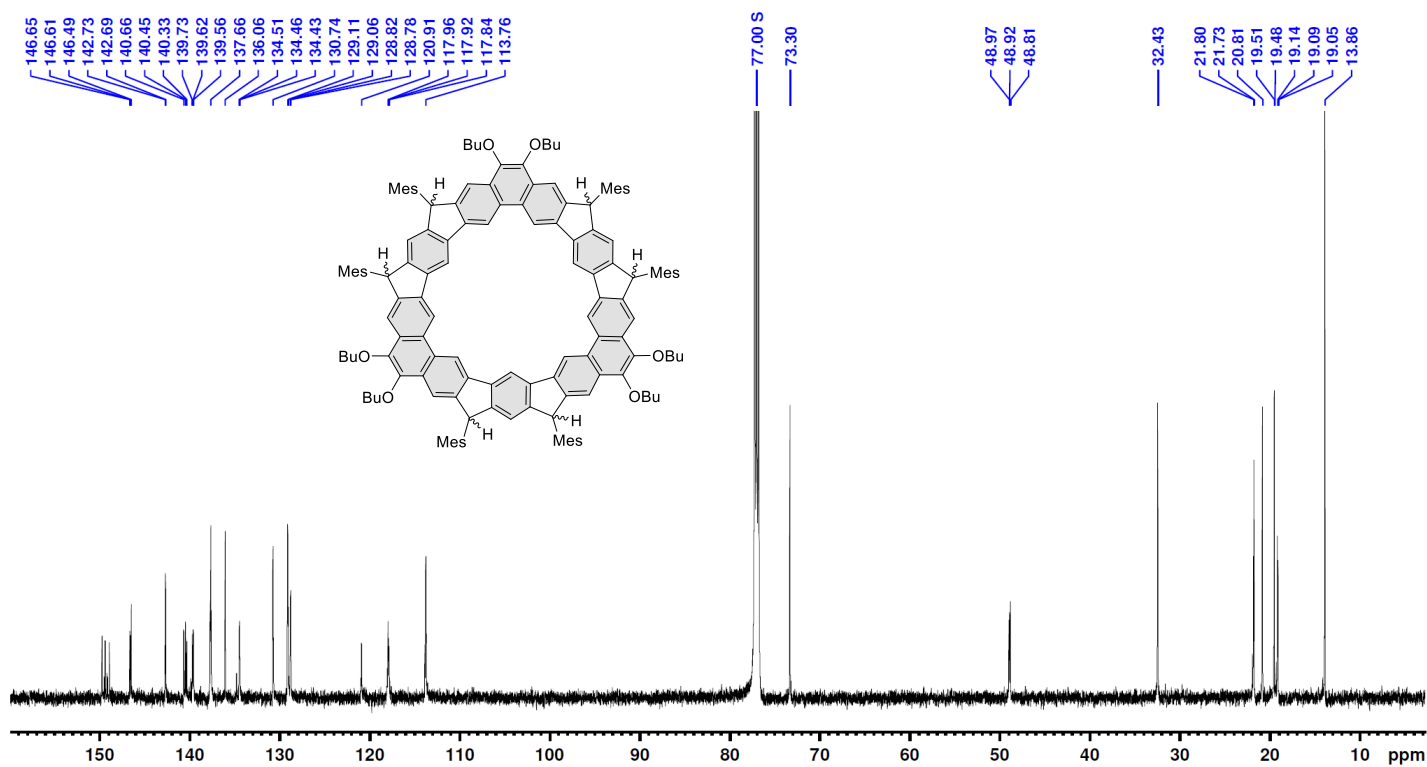**Figure S31.** ^{1}H NMR spectrum of compound **12**(mixture of stereoisomers) (500 MHz, chloroform-*d*, 300 K).

Figure S32. ^{13}C NMR spectrum of compound **12**(mixture of stereoisomers) (125 MHz, chloroform-*d*, 300 K).
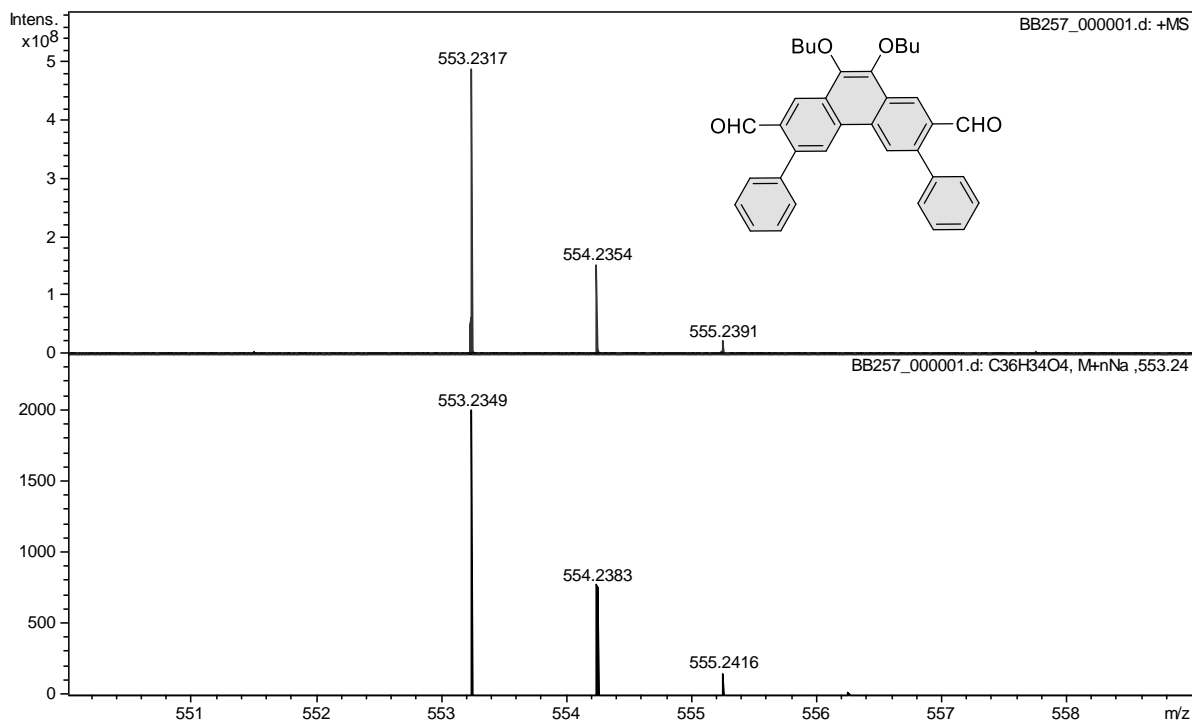
Mass Spectra

Figure S33. High resolution mass spectrum of **S1** (ESI–TOF, top: experimental, bottom: simulated).
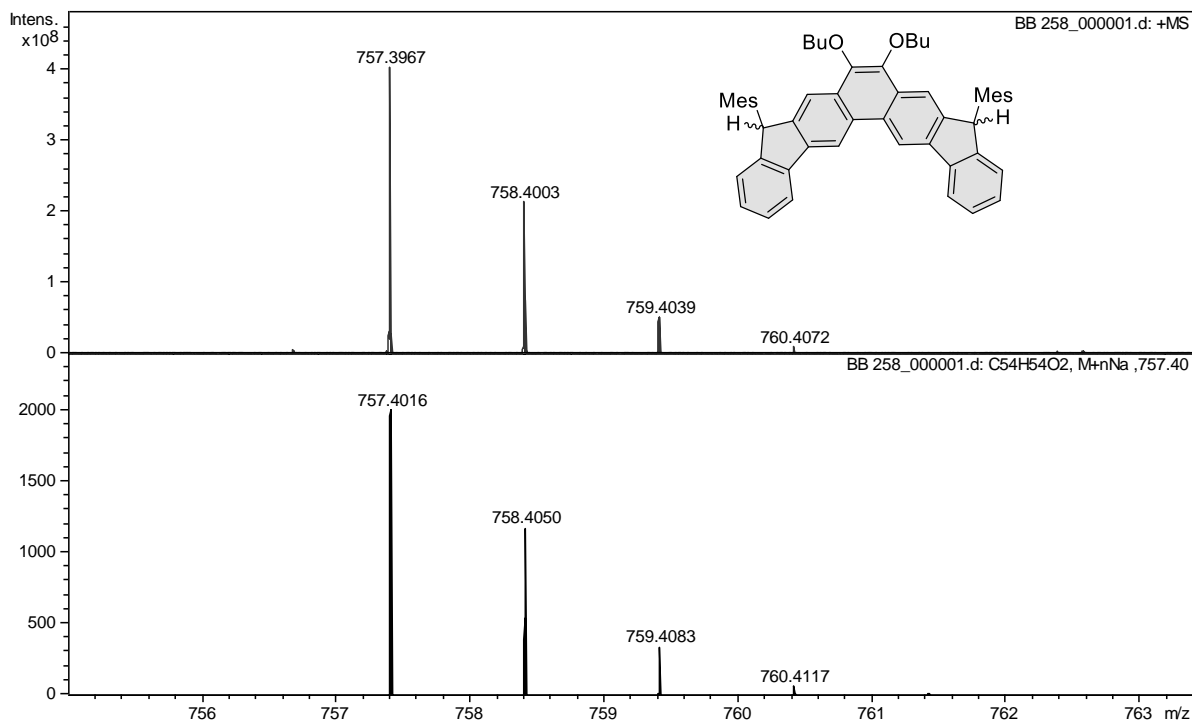

Figure S34. High resolution mass spectrum of **S2** (ESI–TOF, top: experimental, bottom: simulated).
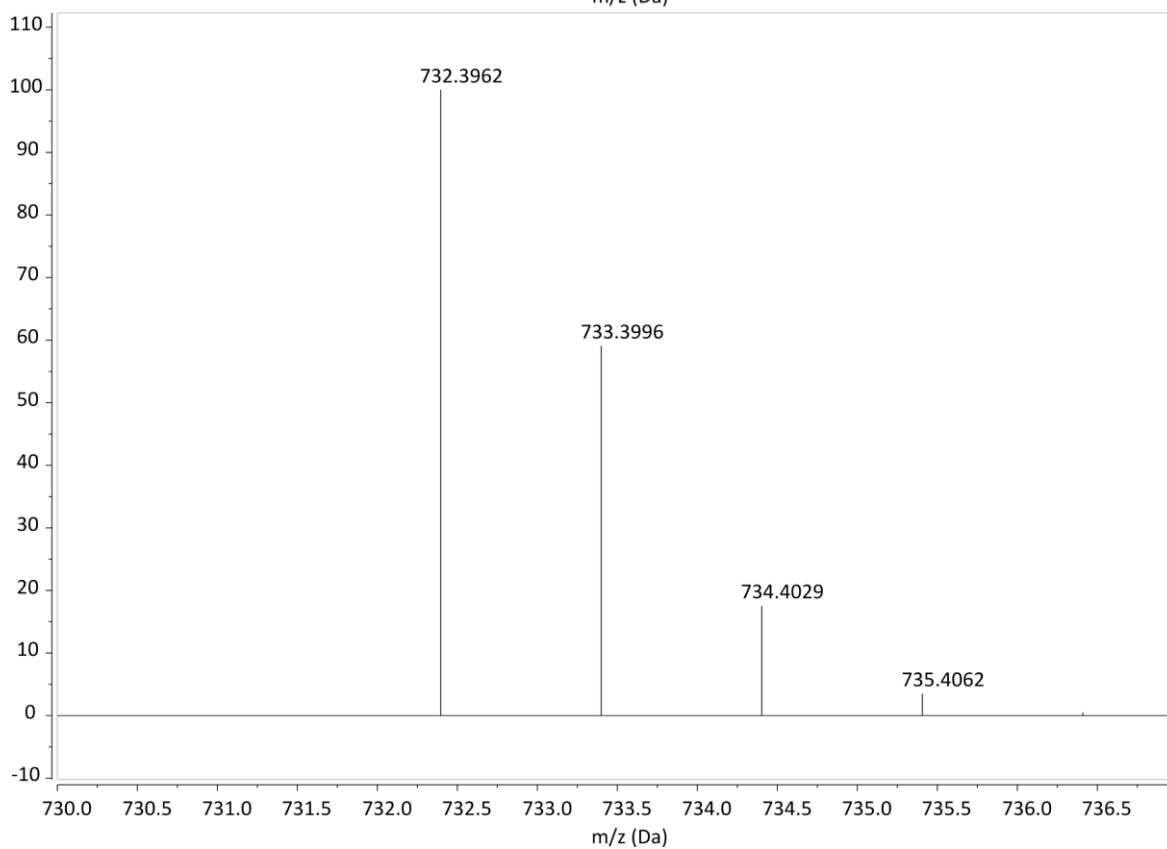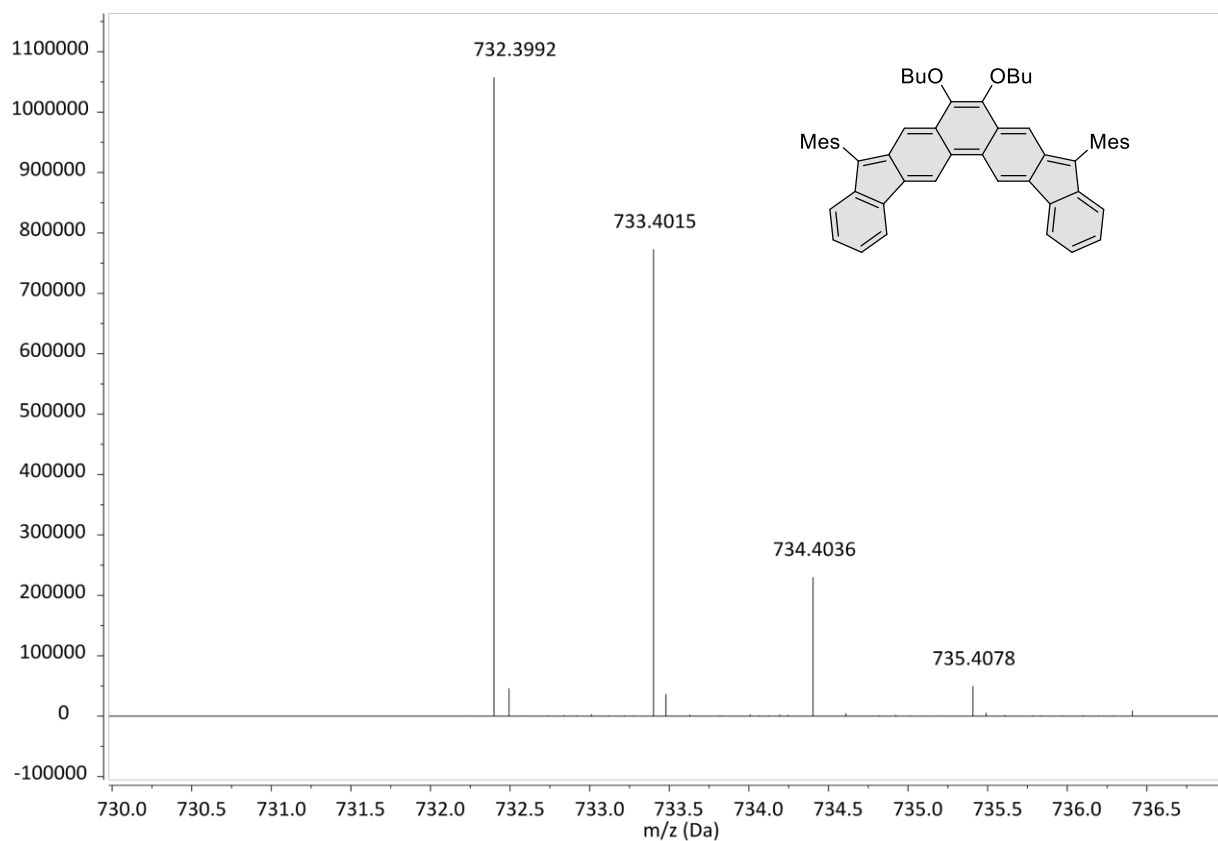
Figure S35. High resolution mass spectrum of **9** (ESI–TOF, top: experimental, bottom: simulated).
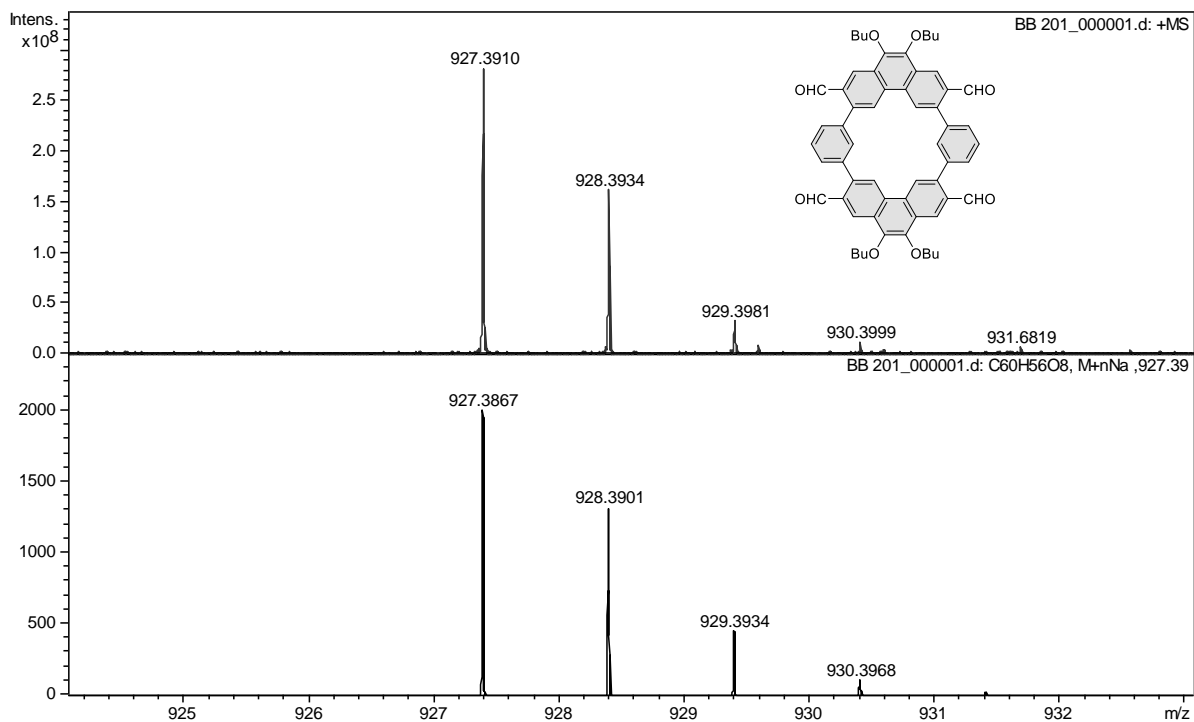
Figure S36. High resolution mass spectrum of **11a** (ESI–TOF, top: experimental, bottom: simulated).
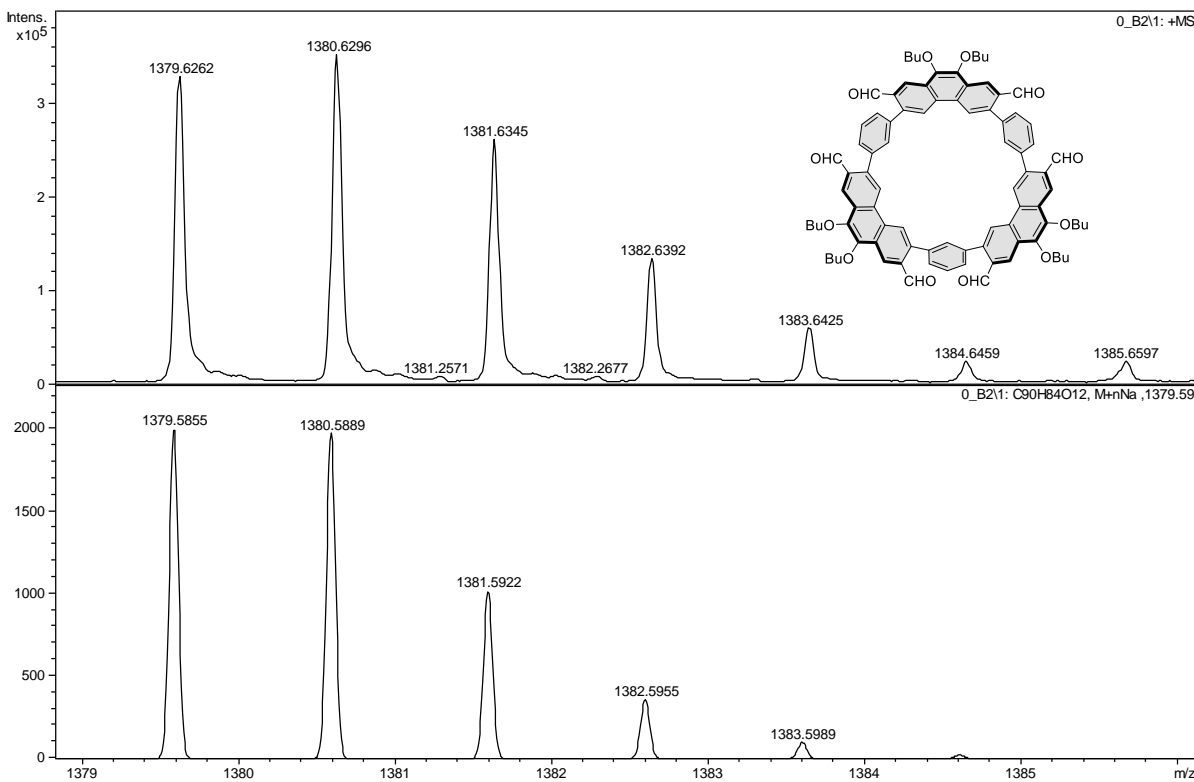

Figure S37. High resolution mass spectrum of **11b** (MALDI–TOF, top: experimental, bottom: simulated).
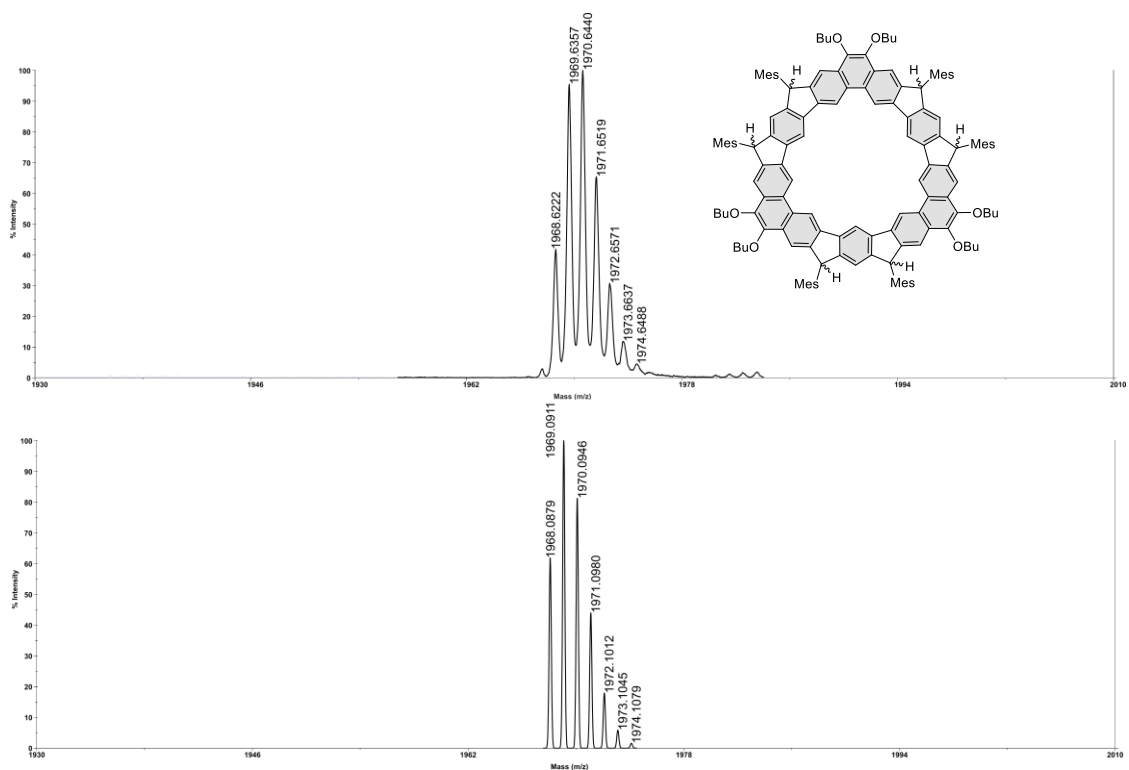
Figure S38. High resolution mass spectrum of **12** (MALDI–TOF, top: experimental, bottom: simulated).
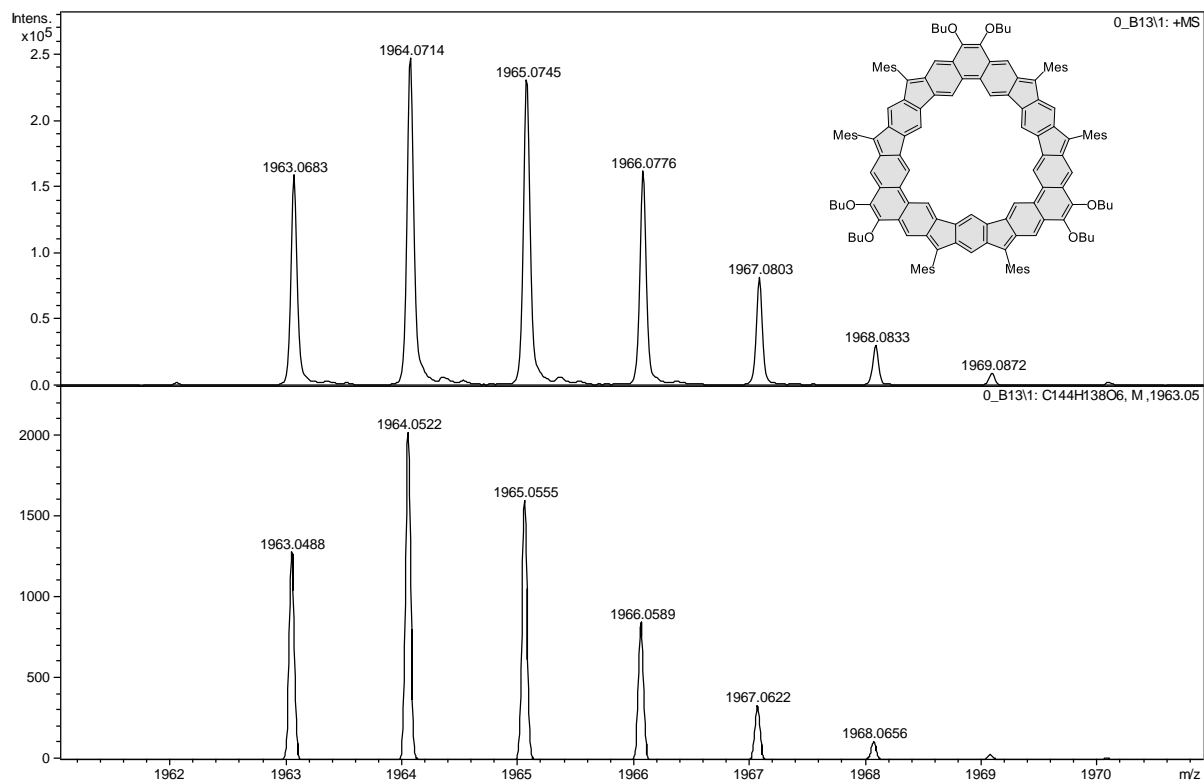

Figure S39. High resolution mass spectrum of **8** (MALDI–TOF, top: experimental, bottom: simulated).

References

(1)   Gregolińska, H.; Majewski, M.; Chmielewski, P. J.; Gregoliński, J.; Chien, A.; Zhou, J.; Wu, Y.-L.; Bae, Y. J.; Wasielewski, M. R.; Zimmerman, P. M.; Stępień, M. Fully Conjugated [4]Chrysaorene. Redox-Coupled Anion Binding in a Tetraradicaloid Macrocycle. *J. Am. Chem. Soc.* **2018**, 140 (43), 14474–14480. https://doi.org/10.1021/jacs.8b09385.

(2)   Bain, G. A.; Berry, J. F. Diamagnetic Corrections and Pascal's Constants. *J. Chem. Educ.* **2008**, 85 (4), 532. https://doi.org/10.1021/ed085p532.

(3)   Frisch, M. J.; Trucks, G. W.; Schlegel, H. B.; Scuseria, G. E.; Robb, M. A.; Cheeseman, J. R.; Scalmani, G.; Barone, V.; Petersson, G. A.; Nakatsuji, H.; Li, X.; Caricato, M.; Izmaylov, A. F.; Zheng, G.; Sonnenberg, J. L.; Hada, M.; Ehara, M.; Toyota, K.; Fukuda, R.; Hasegawa, J.; Ishida, M.; Nakajima, T.; Honda, Y.; Kitao, O.; Nakai, H.; Vreven, T.; Montgomery, Jr., J. A.; Peralta, J. E.; Ogliaro, F.; Bearpark, M.; Heyd, J. J.; Brothers, E.; Kudin, K. N.; Staroverov, V. N.; Kobayashi, R.; Normand, J.; Raghavachari, K.; Rendell, A.; Burant, J. C.; Iyengar, S. S.; Tomasi, J.; Cossi, M.; Millam, J. M.; Klene, M.; Adamo, C.; Gomperts, R.; Stratmann, R. E.; Yazyev, O.; Austin, A. J.; Cammi, R.; Pomelli, C.; Ochterski, J. W.; Martin, R. L.; Morokuma, K.; Zakrzewski, V. G.; Voth, G. A.; Salvador, P.; Dannenberg, J. J.; Dapprich, S.; Daniels, A. D.; Farkas, O.; Foresman, J. B.; Fox, D. J. *Gaussian* 16*, Revision B.*01; Wallingford CT, 2016.

(4)   Becke, A. D. Density-Functional Exchange-Energy Approximation with Correct Asymptotic Behavior. *Phys. Rev. A* **1988**, 38 (6), 3098–3100.

(5)   Becke, A. D. Density-functional Thermochemistry. III. The Role of Exact Exchange. *J. Chem. Phys.* **1993**, 98 (7), 5648–5652. https://doi.org/10.1063/1.464913.

(6)   Lee, C.; Yang, W.; Parr, R. G. Development of the Colle-Salvetti Correlation-Energy Formula into a Functional of the Electron Density. *Phys. Rev. B* **1988**, 37 (2), 785–789. https://doi.org/10.1103/PhysRevB.37.785.

(7)   Yanai, T.; Tew, D. P.; Handy, N. C. A New Hybrid Exchange–Correlation Functional Using the Coulomb-Attenuating Method (CAM-B3LYP). *Chem. Phys. Lett.* **2004**, 393 (1–3), 51–57. https://doi.org/10.1016/j.cplett.2004.06.011.

(8)   Grimme, S.; Ehrlich, S.; Goerigk, L. Effect of the Damping Function in Dispersion Corrected Density Functional Theory. *J. Comput. Chem.* **2011**, 32 (7), 1456–1465. https://doi.org/10.1002/jcc.21759.

(9)   Herges, R.; Geuenich, D. Delocalization of Electrons in Molecules [†]. *J. Phys. Chem. A* **2001**, 105 (13), 3214–3220. https://doi.org/10.1021/jp0034426.

(10)   Geuenich, D.; Hess, K.; Köhler, F.; Herges, R. Anisotropy of the Induced Current Density (ACID), a General Method To Quantify and Visualize Electronic Delocalization. *Chem. Rev.* **2005**, 105 (10), 3758–3772. https://doi.org/10.1021/cr0300901.

(11)   Roos, B. O. The Complete Active Space SCF Method in a Fock-Matrix-Based Super-CI Formulation. *Int. J. Quantum Chem.* **1980**, 18 (S14), 175–189. https://doi.org/10.1002/qua.560180822.

(12)   Roos, B. O.; Taylor, P. R.; Sigbahn, P. E. M. A Complete Active Space SCF Method (CASSCF) Using a Density Matrix Formulated Super-CI Approach. *Chem. Phys.* **1980**, 48 (2), 157–173. https://doi.org/10.1016/0301-0104(80)80045-0.

(13)   Aquilante, F.; Pedersen, T. B.; Lindh, R. Low-Cost Evaluation of the Exchange Fock Matrix from Cholesky and Density Fitting Representations of the Electron Repulsion Integrals. *J. Chem. Phys.* **2007**, 126 (19), 194106. https://doi.org/10.1063/1.2736701.

(14)   Boström, J.; Aquilante, F.; Pedersen, T. B.; Lindh, R. Ab Initio Density Fitting: Accuracy Assessment of Auxiliary Basis Sets from Cholesky Decompositions. *J. Chem. Theory Comput.* **2009**, 5 (6), 1545–1553. https://doi.org/10.1021/ct9000284.

(15)   Fdez. Galván, I.; Vacher, M.; Alavi, A.; Angeli, C.; Aquilante, F.; Autschbach, J.; Bao, J. J.; Bokarev, S. I.; Bogdanov, N. A.; Carlson, R. K.; Chibotaru, L. F.; Creutzberg, J.; Dattani, N.; Delcey, M. G.; Dong, S. S.; Dreuw, A.; Freitag, L.; Frutos, L. M.; Gagliardi, L.; Gendron, F.; Giussani, A.; González, L.; Grell, G.; Guo, M.; Hoyer, C. E.; Johansson, M.; Keller, S.; Knecht, S.; Kovačević, G.; Källman, E.; Li Manni, G.; Lundberg, M.; Ma, Y.; Mai, S.; Malhado, J. P.; Malmqvist, P. Å.; Marquetand, P.; Mewes, S. A.; Norell, J.; Olivucci, M.; Oppel, M.; Phung, Q. M.; Pierloot, K.; Plasser, F.; Reiher,

M.; Sand, A. M.; Schapiro, I.; Sharma, P.; Stein, C. J.; Sørensen, L. K.; Truhlar, D. G.; Ugandi, M.; Ungur, L.; Valentini, A.; Vancoillie, S.; Veryazov, V.; Weser, O.; Wesołowski, T. A.; Widmark, P.-O.; Wouters, S.; Zech, A.; Zobel, J. P.; Lindh, R. OpenMolcas: From Source Code to Insight. *J. Chem. Theory Comput.* **2019**, 15 (11), 5925–5964. https://doi.org/10.1021/acs.jctc.9b00532.

(16) Zimmerman, P. M.; Bell, F.; Goldey, M.; Bell, A. T.; Head-Gordon, M. Restricted Active Space Spin-Flip Configuration Interaction: Theory and Examples for Multiple Spin Flips with Odd Numbers of Electrons. *J. Chem. Phys.* **2012**, 137 (16), 164110. https://doi.org/10.1063/1.4759076.

(17) Bell, F.; Zimmerman, P. M.; Casanova, D.; Goldey, M.; Head-Gordon, M. Restricted Active Space Spin-Flip (RAS-SF) with Arbitrary Number of Spin-Flips. *Phys Chem Chem Phys* **2013**, 15 (1), 358–366. https://doi.org/10.1039/C2CP43293E.

(18) Dai, D.; Whangbo, M.-H. Spin Exchange Interactions of a Spin Dimer: Analysis of Broken-Symmetry Spin States in Terms of the Eigenstates of Heisenberg and Ising Spin Hamiltonians. *J. Chem. Phys.* **2003**, 118 (1), 29–39. https://doi.org/10.1063/1.1525809.

(19) Majewski, M. A.; Chmielewski, P. J.; Chien, A.; Hong, Y.; Lis, T.; Witwicki, M.; Kim, D.; Zimmerman, P. M.; Stępień, M. 5,10-Dimesityldiindeno[1,2-a:2′,1′-i]Phenanthrene: A Stable Biradicaloid Derived from Chichibabin's Hydrocarbon. *Chem. Sci.* **2019**, 10 (11), 3413–3420. https://doi.org/10.1039/C9SC00170K.